

**RESPONSE OF A RESIDENTIAL STRUCTURE AND  
BURIED PIPELINES TO CONSTRUCTION BLASTING IN  
BASALT ON THE WEST SIDE OF ALBUQUERQUE - NM**

by

Vitor Luconi Rosenhaim

Advisor: Dr. Catherine Aimone – Martin

Submitted in partial fulfillment of the requirement for the  
Degree of Master of Science in Mineral Engineering with Specialization in  
Explosives Engineering

Department of Mineral Engineering  
New Mexico Institute of Mining and Technology  
Socorro, New Mexico

September 2005

This thesis is accepted on behalf of the faculty of the  
Institute by the following committee:

---

Academic Advisor

---

Research Advisor

---

Committee Member

---

Committee Member

---

Date

I release this document to New Mexico Institute of Mining and Technology

---

Student signature

Date

## ABSTRACT

The responses of a residential structure and two buried pipelines adjacent to a construction blasting site were monitored. Crack and structure motions were measured in a wood-frame house with a stucco exterior at distances from the blasting between 962 ft to 1208 ft, producing maximum peak particle velocities (PPV) and airblast over pressures (AB) of 0.365 ips and 123 dB, respectively. Blasts were between 57 ft and 201 ft from the pipelines and produced maximum PPV and AB of 5.08 ips and 140 dB, respectively. Whole structural and mid-wall motions were measured at upper and lower corners and on two mid-walls using single-axis velocity transducers. Dynamic and weather-induced changes in the width of an existing exterior stucco crack were recorded. Dynamic structure and crack motions during blasting were time-correlated with ground vibrations and airblast. Wall strains generated during out-of-plane bending and in-plane shear were computed and compared with failure strains for drywall and stucco. Long-term crack movement with variations in temperature and humidity were compared with dynamic peak motions during blasting

The response to blasting of two parallel pipelines with 12 in and 20 in diameters was measured in two areas at the construction site. Each pipeline was instrumented with single axis geophones mounted to record radial (R), vertical (V), and transverse (T) components. The maximum longitudinal, circumferential (hoop), and bending stresses were computed using elastic strain equations for the highest amplitude pipeline response.

Structures responses were correlated with PPV and AB, that arrived simultaneously, which complicated the distinction between the two. Calculated strains were far lower than those required to crack drywall. Environmentally induced crack

response from temperature and humidity was far greater than that caused by blast induced ground motion or airblast overpressures. The highest value of the calculated hoop stress for the two pipelines was found to be smaller than the recommended maximum hoop stresses, determining that all blasting that took place close to the pipelines was safe. It was demonstrated using the flexibility ratio and comparing the pipeline amplitudes that the larger diameter pipeline is more flexible than the smaller diameter pipeline. It was recommended that the maximum peak ground velocity at the pipelines should be at 9.73 ips.

## ACKNOWLEDGEMENTS

I would like to thank the following people for their time and dedication on this project.

- Dr. Aimone-Martin
- Jhon White from Salls Brothers Construction, Inc
- Dr. Mojtabi
- Dr. Fakhimi
- Dr. Dowding
- Meghan Vallejo
- Courtney Vallejo
- Tye Lasich
- Farid Sarioseri and all the other students that assisted with field work and data analyses

I would also like to thank my family and friends that even been far away in Brazil have been supporting me in this endeavor.

## TABLE OF CONTENTS

LIST OF TABLES .....	vii
LIST OF FIGURES .....	viii
1 INTRODUCTION .....	1
1.1 Background.....	1
1.2 Site Description.....	2
1.3 Scope.....	2
2 STRUCTURE RESPONSE .....	6
2.1 Velocity Time Histories Measurements.....	7
2.2 Natural Frequency and Damping Ratio .....	8
2.3 Upper Structure Amplification of Ground Velocities.....	12
2.4 Strain Calculations .....	14
2.5 Crack Response to Static and Dynamic Forces .....	16
2.5.1 Long-Term Environmental and Weather-induced Crack Response .....	16
2.5.2 Crack Response to Blasting .....	17
3 PIPELINE RESPONSE .....	18
3.1 Allowable Stress in Pipelines.....	19
3.2 Blasting Vibration Criteria for Pipelines .....	21
3.3 Procedures to Estimate Strains and Stresses in Pipeline from Velocity Measurements .....	24
4 INSTRUMENTATION .....	28
4.1 Structure Vibrations .....	28
4.2 Crack Displacements .....	31
4.3 Pipeline Response .....	34

4.3.1	Instrumentation Design and Implementation.....	34
4.4	Data Acquisition and Reduction .....	36
5	CONSTRUCTION BLAST DESIGNS .....	37
5.1	Blasting Patterns .....	37
5.2	Wave Propagation Velocity Measurement .....	39
6	RESULTS .....	41
6.1	Ground Motion and Airblast Characteristics .....	41
6.2	Structure Response to Blasting .....	44
6.2.1	Comparison of Structure Response with Ground Motions and Airblast ..	45
6.2.2	Natural Frequency and Damping Ratio .....	53
6.2.3	Upper Structure Amplification of Ground Velocities.....	54
6.2.4	Strains Calculated for Structure Walls.....	55
6.2.5	Crack Response.....	57
6.3	Pipeline Response .....	65
6.3.1	Response of Pipelines .....	68
6.3.2	Response Ratio of Pipeline Relative to Ground Motion.....	70
6.3.3	Estimation of Strains and Stresses in Pipelines .....	71
7	CONCLUSIONS AND RECOMMENDATIONS .....	78
8	REFERENCES .....	84
	APPENDIX A - Seismograph Reports for Ground Vibration and Airblast .....	86
	APPENDIX B - Seismograph Reports for Structure Response.....	119
	APPENDIX C - Seismograph Reports for Pipeline Response.....	153
	APPENDIX D - Summary Tables of all Seismograph Data.....	199

APPENDIX E - Maps and Layouts of each Blast.....	202
APPENDIX F - Summary Table of all Velocity and Airblast Data for the Seismographs in the house.....	216
APPENDIX G - Velocity Time Histories Comparative Plots.....	219
APPENDIX H - Displacement time Histories used to Compute Strains.....	231
APPENDIX I - Crack Displacement Time Histories.....	249

## LIST OF TABLES

Table 3.1 Summary of vibration limits imposed in representative coal mining states <sup>(1)</sup> ..	23
Table 5.1 Summary of blast designs used during the response study (PPV on the ground) .....	38
Table 6.1 Summary of blasting data, ground motion and airblast in the structure .....	45
Table 6.2 Summary of structure response for the east wall.....	46
Table 6.3 Summary of structure response for the north wall.....	46
Table 6.4 Summary of natural frequency and percentage of damping for the structure .	53
Table 6.5 Summary of upper structure amplification of ground velocities .....	54
Table 6.6 Whole structure in-plane and mid-wall strains induced by ground motion excitation and compared with crack peak displacements .....	55
Table 6.7 Peak crack displacement compared with ground velocity (GV), airblast, differential wall displacement (upper, S2, minus lower ,S1, structure) and mid-wall (MW) displacement .....	60
Table 6.8 Summary of vibration measurements in the pipelines.....	66
Table 6.9 Response ratio of pipelines relative to surface motions .....	71

## LIST OF FIGURES

Figure 1.1	Picture showing the location of the site and structures .....	3
Figure 1.2	Views from each side of the house.....	4
Figure 1.3	Gas pipelines views, (a) looking down into the excavation, X-42 pipelines, 12 in (top) and 20 in (bottom) and (b) X-52 same diameters .....	4
Figure 2.1	Position of transducers used to measure the structure response.....	7
Figure 2.2	Methods used to determine structure natural frequency (a) free response and (b) 90 degree phase match .....	10
Figure 2.3	Upper structure radial component (east wall) free response time history (above) and the FFT for the free response showing the predominant frequency (below), for the blast at 09/16/04.....	11
Figure 2.4	Time correlated ground velocity and upper structure response waveforms used to determine amplification factor (data from blast at 01/27/05a).....	13
Figure 2.5	Global shear strain in the wall.....	15
Figure 2.6	Wall geometry used to estimate in-plane tensile wall strains.....	16
Figure 3.1	Location of pipelines .....	18
Figure 3.2	(a) Longitudinal, $\varepsilon_l$ and (b) circumferential, $\varepsilon_c$ , and (c) bending, $\varepsilon_b$ , strain components of pipeline deformations.....	24
Figure 4.1	Schematic plan view of the resident showing the location of the single velocity component transducers and the crack gauge.....	29
Figure 4.2	Location of velocity transducers to measure structure response in the walls. 29	
Figure 4.3	Details of velocity transducers locations in the (a) upper (S2) and (b) lower (S1) corner .....	30
Figure 4.4	Location of Kaman gages and SOMAT field computer on the east wall of the structure.....	32
Figure 4.5	Close up in the gage active element (left) and brackets mounted in an existing crack (right).....	32
Figure 4.6	Displacement gage system used to measure opening and closing of an existing crack.....	33

Figure 4.7 Section (looking west) and plan views showing the location of the velocity sensors on the pipelines .....	35
Figure 4.8 Attached single component transducers to the pipeline top, components V and T and to the side facing the blast, component R, for (a) 12 in X-42 pipeline and (b) 20 in X-42 pipeline .....	35
Figure 5.1 Construction blast designs, road cut (left) and utility trench (right) .....	38
Figure 5.2 Trench blast been covered with sand.....	39
Figure 5.3 Seismograph array used to measure wave speed velocity in the ground .....	40
Figure 5.4 Wave speed in the ground .....	40
Figure 6.1 Peak particle velocity in the ground versus scaled distance for the attenuation study, the data is divided by date of the blast .....	42
Figure 6.2 Peak airblast versus cube-root scaled distance for the attenuation study .....	42
Figure 6.3 Velocity time histories comparisons of (a) east and (b) north ground motion (GV), lower corner (S1), upper corner (S2), mid-walls (MW), and airblast for the structure, first blast at 12/30/04 .....	47
Figure 6.4 Velocity time histories comparisons of (a) east and (b) north ground motion (GV), lower corner (S1), upper corner (S2), mid-walls (MW), and airblast for the structure, first blast at 01/27/05 .....	48
Figure 6.5 Ground velocity influence on peak motion of the upper structure corners for (a) radial and (b) transverse ground components.....	50
Figure 6.6 Ground velocity influence on peak mid-wall velocity for (a) radial ground velocity versus east mid-wall and (b) transverse ground velocity versus north mid-wall.....	51
Figure 6.7 Airblast overpressure influence on mid-wall response .....	51
Figure 6.8 Peak airblast overpressure influence on upper structure (S2) velocity for (a) radial and (b) transverse components .....	52
Figure 6.9 Influence of (a) transverse and (b) radial ground motions on calculated in-plane strains .....	56
Figure 6.10 Influence of (a) radial and (b) transverse ground motions on calculated mid-wall bending strains .....	57

Figure 6.11 Static changes of crack width to variations in temperature and humidity over 135 days .....	58
Figure 6.12 Variations in data over 22 days showing the change in crack width (positive indicated crack is opening) from early morning to mid-day.....	59
Figure 6.13 Composite waveforms, comparing crack displacement time histories with ground motion in R and T directions, airblast, upper structure east and north wall displacement and mid-wall displacement in the east wall .....	61
Figure 6.14 Peak dynamic crack displacement versus (a) radial and (b) transverse components of ground motions, versus maximum (S2 – S1) differential displacement (c) perpendicular and (d) parallel with east wall, and versus (e) maximum air overpressure, time correlated.....	63
Figure 6.15 Comparison of dynamic crack displacement time history for blast on 12/30/04 with static crack movement in response to climate over a 25 day period including 12/30/04 .....	64
Figure 6.16 Pipeline response data plotted with the peak particle velocity of ground motion .....	67
Figure 6.17 Comparison of vertical components for ground surface and pipelines grouped in respect to the orientation with the blast initiation.....	68
Figure 6.18 Comparison of transverse components for ground surface and pipelines grouped in respect to the orientation with the blast initiation.....	69
Figure 6.19 Comparison of radial components for ground surface and pipelines grouped in respect to the orientation with the blast initiation.....	69

# 1 INTRODUCTION

## 1.1 Background

Blast vibration monitoring and analysis were conducted at the Unser road extension near a construction site in the northwest part of Albuquerque, NM. The purpose of this study is to characterize the dynamic structure response of a house and two pipelines to blasting. The construction site, operate by Salls Brothers Construction, Inc., is located at distances between 758 ft to 1625 ft to the east of the house and at distances between 50 ft to 206 ft to the north and northeast of the two pipelines. Over a four and one-half month period, whole structure vibrations were recorded using velocity and air pressure transducers during ground motion and airblast excitations produced by blasting activities. A pre-existing exterior crack in the stucco on the east wall of the house was monitored for displacement. Structure instrumentation employed in this study included an exterior tri-axial velocity geophone and airblast microphone, interior single component velocity transducers mounted at the upper and lower northeast wall corner and north and east mid-walls, Kaman eddy-current displacement gages affixed over the exterior wall crack, single component velocity transducers mounted at the side and top of the pipelines, and tri-axial velocity geophones and airblast microphones installed in the ground above the pipelines.

Vibration levels and crack displacements were monitored to determine the effects of construction blasting on the house and the pipelines. In addition, dynamic crack displacements measured during blasting were compared with static (long-term) changes

in the crack width in response to changes in ambient temperature and humidity. Instrumentation was installed at the house on 9/16/04 to monitor the effects from 12 blasts, and at the pipelines on 9/21/04 to monitor the effects from 9 blasts over the project duration, and was removed on 2/13/05.

Blasting was conducted on two different patterns that included trench and road blasts, rectangular in shape and initiated using non-electric detonators. ANFO (ammonium-nitrate fuel-oil) was used as the primary explosive. Between 20 and 360 blastholes, of 3.0 in diameter, were used per shot. The explosive weight detonated within an 8-millisecond (ms) delay ranged from 3 to 216 lbs. This parameter is of special importance as it affects the magnitude of off-site ground vibrations.

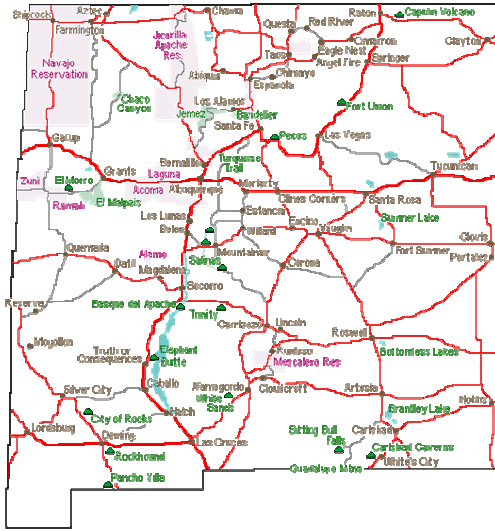
## **1.2 Site Description**

The site location and identification of the residential structure are shown in Figure 1.1. The construction site where the structures are located includes a residential development area and extension to Unser road. The house, shown in Figure 1.2, is a single-story, slab-on-grade wood-framed structure with stucco exterior. The X-42 and X-52 gas pipelines at the site are 12 in and 20 in in diameter, respectively, and located at the southeast and northwest regions of the site as shown in Figure 1.3. The southeast lines were removed during the project and replaced by the lines at the northwest location.

## **1.3 Scope**

Chapters 2 and 3 describe the procedures used to analyze structure response of the house and pipelines, respectively, to construction blasting. Chapter 4 presents the procedures to instrument the structure and pipelines. Construction blast designs and wave

speed analysis are given in Chapter 5 and results are presented in Chapter 6. Conclusions and references are given in Chapter 7 and 8, respectively. Appendices contain the following:



(a)



(b)

Figure 1.1 Picture showing the location of the site and structures



Figure 1.2 Views from each side of the house



(a)

(b)

Figure 1.3 Gas pipelines views, (a) looking down into the excavation, X-42 pipelines, 12 in (top) and 20 in (bottom) and (b) X-52 same diameters

#### Appendix

A Seismograph reports for ground vibration and airblast

B Seismograph reports for structure response

C Seismograph reports for pipeline response

D Summary table of all seismograph data

E Maps and layouts of each blast

F Summary table of all velocity and airblast data values for the seismographs in the house

- G Velocity time histories comparative plots
- H Displacement time histories used to compute strains
- I Crack displacement time histories

## 2 STRUCTURE RESPONSE

Whole structure and mid-wall structure motions were measured using single-axis velocity geophones. A single tri-axial geophone, buried in the ground, and an air pressure sensor are employed in the exterior of the residence to record ground motions and airblast. Displacement type gages are used to measure the motions of an existing exterior wall crack. These instruments are used to record blast-induced motions and the data is analyzed to:

- compare vibration time histories in terms of velocity and calculated displacements within structures relative to ground excitations and air overpressures,
- evaluate response frequencies to determine natural frequencies and damping characteristics,
- determine structure response amplification of ground motions,
- compute differential displacements at corner motions to estimate global shear and in-plane tension wall strains, and
- compute bending strains in walls.

Corner and mid-wall motions from blasting were compared with motions induced crack width changes. Further, the crack responses (e.g., crack opening and closing) to variations in ambient temperature and humidity were recorded.

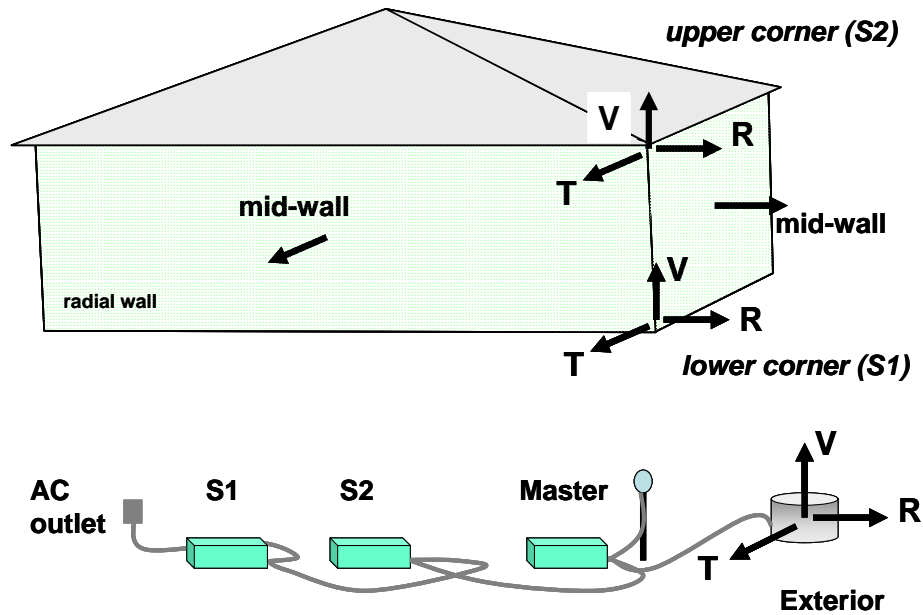


Figure 2.1 Position of transducers used to measure the structure response

## 2.1 Velocity Time Histories Measurements

Figure 2.1 shows the position of transducers used to measure the structure response. The two corner transducers (S2, upper corner, and S1, lower corner) measure whole structure motions in the radial (R), transverse (T), and vertical (V) directions. The mid-wall (MW) transducers measure horizontal motions during wall flexure or bending.

Motions measured by the transducers are stored in form of velocity time histories waveforms. White 2000<sup>TM</sup> software was used to plot the velocity and air pressure time histories, determine the predominate frequency using the Fast Fourier Transform (FFT) analysis, and integrate the velocity to obtain displacement time histories. Two frequencies, or wave cycles (oscillations) per second, are of interest. These include the peak frequency (or frequency at the peak particle velocity, PPV) and the predominant frequency (determined using FFT analysis). The predominant FFT frequency carries the

largest percentage of ground motion energy and is important when evaluating structure response and human perception of vibration from blasting.

Velocity time histories were evaluated to determine the relative amplitude and frequency characteristics among ground velocity (GV), upper (S2) and lower (S1) structure response, and mid-wall (MW) response. Velocity time histories were examined to determine the degree of frequency and phase matching between the exterior excitations and the structure response. The influence of air overpressure on structure motions was also evaluated,

## **2.2 Natural Frequency and Damping Ratio**

Natural frequency is the frequency at which structures oscillate freely after excitation energy is removed or during free response. If the ground vibration arrives at a structure carrying a low predominant frequency component identical to the natural frequency of the structure, the blast wave energy will readily transmit into the structure and start the structure in motion, often amplifying the excitation. The natural frequency match will cause the structure to continue to vibrate for a longer time compared with a ground motion carrying frequencies well above the structure's natural frequency. Fundamental frequencies for whole structure motions typically range from 4 to 12 Hz. Keeping the ground motion frequencies above this range will help minimize the sensation that the structure is being harmed by long duration vibrations when, indeed, the amplitudes are far below those that could cause cracking.

The whole structure natural frequency can be evaluated during free-response, a shift in phase angle between S2 and GV, or using Fast Fourier Transform (FFT) analysis. The free-response method isolates that portion of the upper structure (S2) time history

where ground and air pressure excitations have ceased and the upper structure response decays slowly to zero with a constant frequency. This is illustrated graphically in Figure 2.2 (a). The frequency of this trailing structure response is thought to represent the natural frequency of the structure and may be the best approximation of natural frequencies. Structure free response is best observed when horizontal ground velocities are 0.3 ips or higher for most single-story structures.

Natural frequencies are also observed where the S2 response peaks show a  $90^\circ$  lag behind the excitation (GV) peaks for the same phase (positive or negative peaks) and is illustrated in Figure 2.2 (b). The “phase shift” occurs during the decay portion of the time history (after the maximum) and this portion can be used to estimate the natural frequency. Actual determination of the exact phase angle shift and resulting natural frequency can be calculated using the “zero-crossing” method and the velocity time history. This is computed by taking the  $\frac{1}{2}$  cycle containing the desired peak and dividing by the time difference where the  $\frac{1}{2}$  cycle crosses the time axis.

When neither method can be applied to a given time history, the natural frequency may be estimated by performing a Fast Fourier Transform on the trailing portion of the time history.

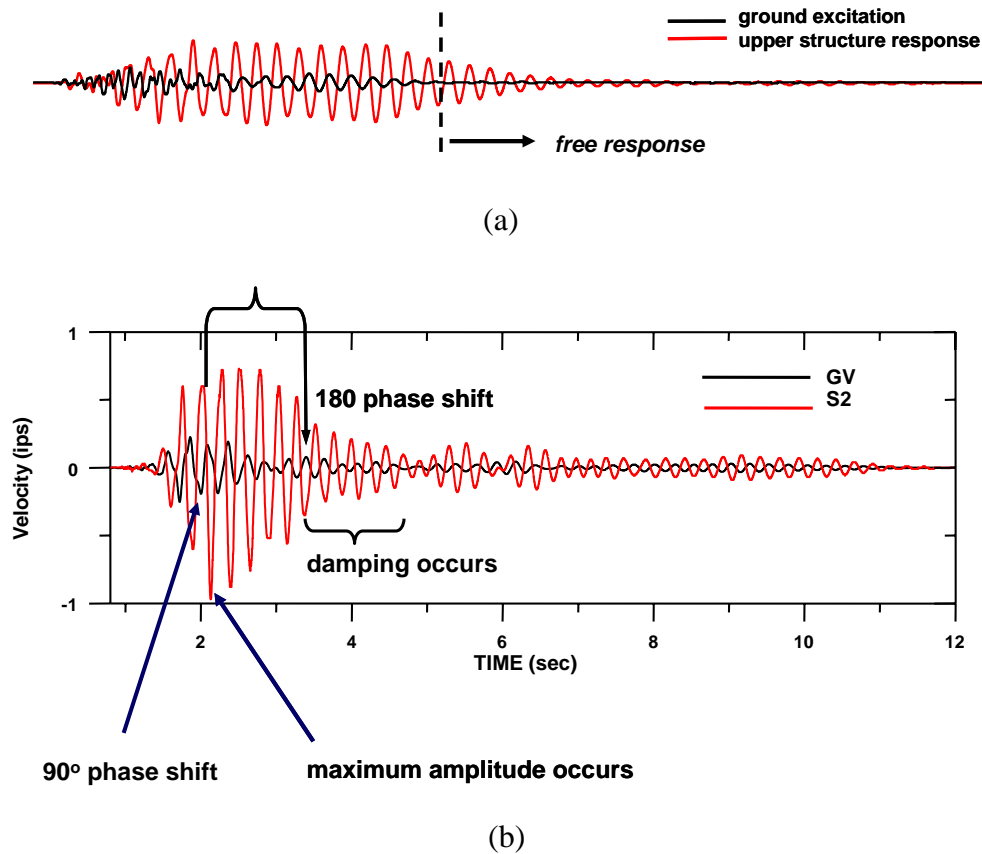


Figure 2.2 Methods used to determine structure natural frequency (a) free response and (b) 90 degree phase match

Damping is a natural phenomenon that occurs in all materials when subjected to an impulse force. Structure motions from excitations (ground velocities) are naturally attenuated or diminished (decays) during energy dissipation and eventually come to rest. The percentage of critical damping,  $\beta$ , is a measure of structure rigidity and how fast the energy of excitation decays in the structure. Damping is calculated using two successive peaks ( $P_1$  and  $P_2$ ) either during free response or during a 90° phase shift, as previously explained.

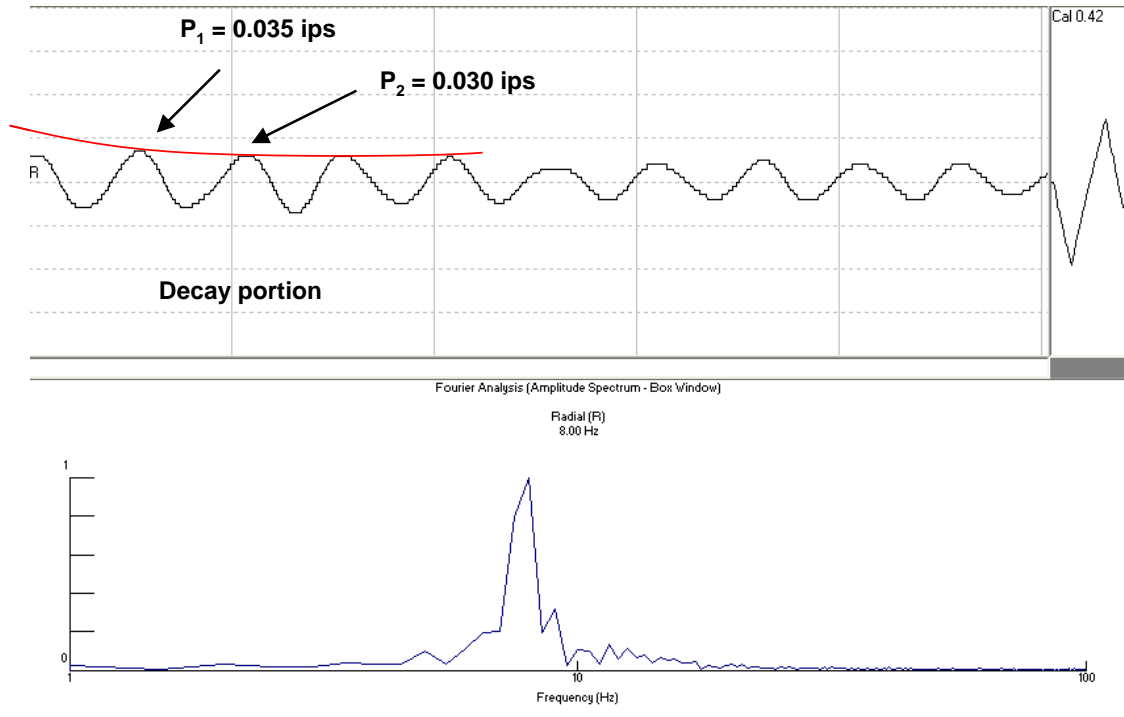


Figure 2.3 Upper structure radial component (east wall) free response time history (above) and the FFT for the free response showing the predominant frequency (below), for the blast at 09/16/04

Two such peaks are shown in Figure 2.3 which represents data from the blast on 09/16/04.

Using P1 and P2, the percentage of critical damping is calculated as follows:

$$\beta = \left( \frac{1}{2\pi} \right) \ln \left( \frac{P_1}{P_2} \right) \quad (1)$$

where,  $\beta$  is the percentage of critical damping (%),  $P_1$  the amplitude of the first peak (ips), and  $P_2$  is the amplitude of the next successive peak (ips).

### 2.3 Upper Structure Amplification of Ground Velocities

Amplification is a comparative measure of the maximum structure response to ground vibration at the same point in time or slightly before the peak at S2, and can be determined in terms of velocity or displacement. It is similar to the term “dynamic amplification factor” used by seismologists to describe the effects of earthquakes on structures.

Amplification occurs when upper corner structure motion at S2 becomes larger than the excitation for the same horizontal component (GV). Amplification factor (AF) was defined for blasting vibrations by the U.S. Bureau of Mines (Siskind, et al., 1980) as the ratio of the peak upper structure velocity ( $S2_{peak}$ ) divided by the preceding ground velocity (GV) of the same phase, positive or negative, that most likely drove the structure peak:

$$AF = \left( \frac{S2_{peak}}{GV} \right) \quad (2)$$

To calculate AF, the time correlated waveforms for the ground (GV) and the upper structures corner ( $S2_{peak}$ ) are displayed in the same window shown in the example in Figure 2.4. The blue line in the figure represents a common time used to locate peaks.

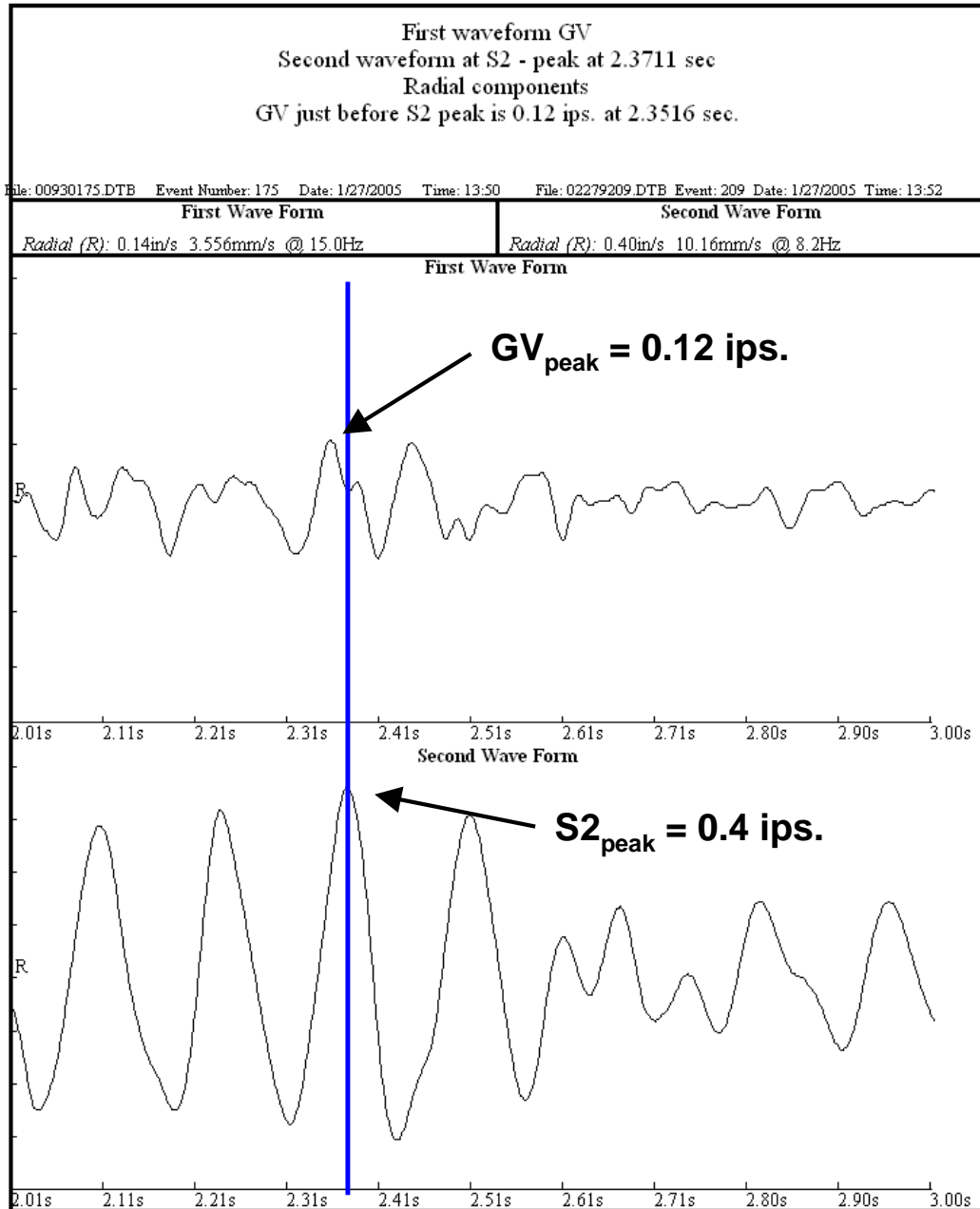


Figure 2.4 Time correlated ground velocity and upper structure response waveforms used to determine amplification factor (data from blast at 01/27/05a)

AF was originally used by the U.S. Bureau of Mines as an indicator of the likelihood of cracking in structures. It was determined by Siskind (1980) and Aimone-Martin, et al., (2003) that typical one- and two-story residential structures will respond to

blasting with AF ranging from less than 1.0 (for very stiff structures) to 4, averaging 2 to 4. However, no direct correlation with crack observations have been reported for AF in excess of 5 that have typically been measured in 2-story and taller structures.

## 2.4 Strain Calculations

The magnitude of induced strains in structure components, as compared to material failure strains, determines the likelihood of cosmetic cracking in residences. Global shear strains may be estimated from differential structure motions calculated in terms of displacements. Calculating displacements entails integrating the velocity time histories at S1 and S2 to obtain displacement time histories and finding the largest time correlated difference between corner responses (S2 minus S1) over the recorded time history. Plots of the differential and component displacements time histories for all blast events are found in Appendix H.

Global, whole structure, shear strain is determined by the following equation and illustrated in Figure 2.5:

$$\gamma_{\max} = \left( \frac{\delta_{\max}}{L} \right) \quad (3)$$

where,  $\gamma_{\max}$  is the global shear strain (micro-strains or  $10^{-6}$  in/in),  $\delta_{\max}$  the maximum differential displacement (S2 – S1), and L is the height of the wall subjected to strain.

In-plane tensile strain,  $\varepsilon_{L\max}$ , is the deformation most likely to cause cosmetic cracking in walls during strong motion and is related to the global shear strain by the equation:

$$\varepsilon_{L_{\max}} = \gamma_{\max} (\sin \theta)(\cos \theta) \quad (4)$$

where,  $\theta$  is the interior angle of the longest diagonal of the wall subjected to strain with reference to a horizontal. Theta,  $\theta$ , is calculated by taking the inverse tangent of the ratio of wall height to wall length as shown in Figure 2.6.

The walls of structures approximate semi-rigid plates which under the influence of excitation tend to flex with maximum magnitude at the middle of the wall. Wall flexure is directly related to bending strains induced in the walls and can be modeled as a beam fixed at both ends, or at the foundation (S1) and at the roof (S2). For structures that are well-coupled to the ground, S1 is “fixed”. However, the roof can be modeled with varying degrees of “coupling”, ranging from relatively unconstrained to highly fixed. Bending strain is best estimated using the fixed-fixed analogy because this model predicts the greatest, strains in walls. This model is given by:

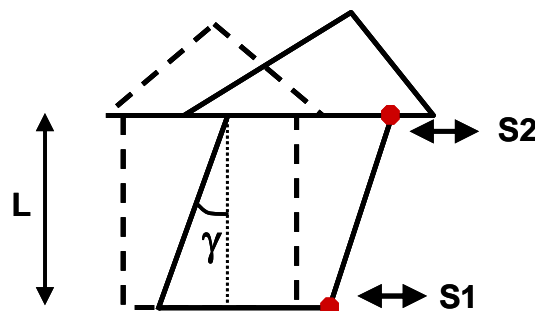


Figure 2.5 Global shear strain in the wall

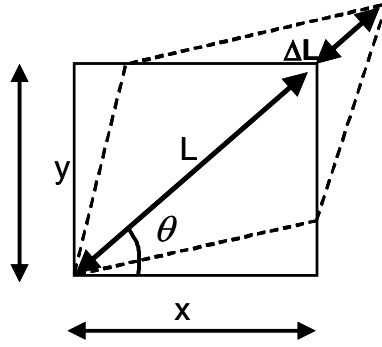


Figure 2.6 Wall geometry used to estimate in-plane tensile wall strains

$$\varepsilon = \left( \frac{6d\Delta\delta_{\max}}{L^2} \right) \quad (5)$$

where,  $\varepsilon$  is the bending strain in walls (micro-strains or  $10^{-6}$ ) and  $d$  is the distance from the neutral axis to the wall surface, or one half the thickness of the wall subjected to strain (in). Note that the wall strains are induced by motions in the wall perpendicular to it. In the case of the studied structure, the transverse component of the GV excitation induced strains in the east wall of the structure, while the radial component of GV induced strains in the north wall.

## 2.5 Crack Response to Static and Dynamic Forces

### 2.5.1 Long-Term Environmental and Weather-induced Crack Response

Variations in the width of wall cracks are highly sensitive to changes in ambient temperature and humidity compared with the dynamic response to blasting. Residents living close to blasting operations may perceive wall cracks as blast-induced. However, it is often the case that blast-induced crack motions are small compared with the static, or

slow, opening and closing of existing cracks with diurnal (or 24-hour) fluctuations in temperature and humidity. To show this comparison, long-term width changes in an exterior stucco crack were measured and recorded on an hourly basis throughout the project. Changes in crack width were then plotted against time for the study structure over the project duration.

In general, crack movement follows a trend in exterior humidity. When humidity increases, the crack opens and this occurs most predominately very early in the mornings before dawn. During the day as temperature increases and humidity decreases, the crack tends to close. It is this daily cycle that produces high stresses at crack tips, promoting slow crack growth over time under the right conditions. The large variation in crack width over a one-half day cycle can be clearly observed.

### **2.5.2 Crack Response to Blasting**

The dynamic response of an existing exterior crack in stucco was measured at the structure during blasting events. Changes in crack widths can be correlated with ground motions and airblast pressures. Also changes in crack widths can be correlated with movement in the walls, by comparing time histories for upper structure (S2) and crack displacements.

### 3 PIPELINE RESPONSE

The pipeline response study was conducted using two parallel pipelines, with diameters of 12 in and 20 in, at two different locations at the construction site as shown in Figure 3.1. In the southeast (SE) part of the site the pipelines were type X-52, with a specified minimum yield strength (SMYS) of 52,000 psi, and a wall thickness of 0.25 in. These pipelines were buried at depths of 3 ft (20 in) and 4 ft (12 in). At the northwest (NW) side of the site, the pipelines were type X-42, with a SMYS of 42,000 psi, and wall thickness of 0.25 in. These pipes are buried at a depth of 6 ft and all pipelines operated at a 400 psi pressure.

The response of buried foundations subjected to continuous vibrations has been the subject of extensive research (Richard, 1970). Foundation design methods used

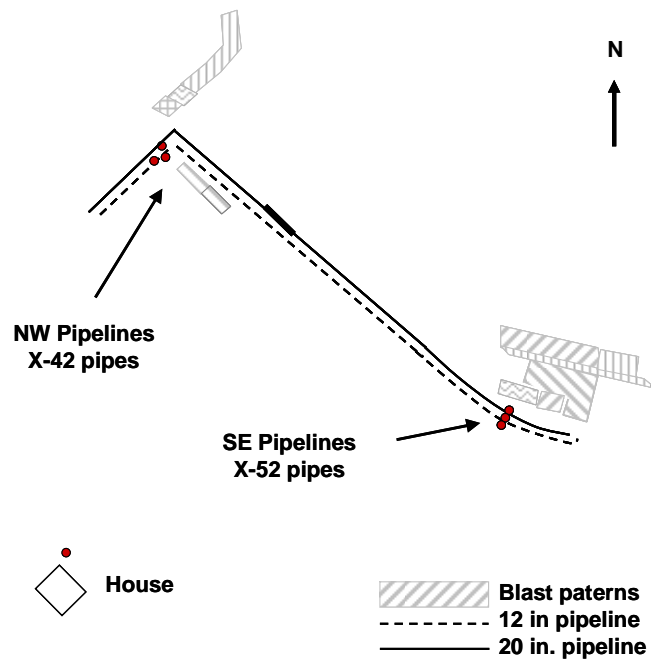


Figure 3.1 Location of pipelines

to ensure that vibration frequencies do not match foundation natural frequencies are well understood. Buried structures response to transient loads for structures such as pipelines has, for the most part, been restricted to earthquake loading. Limited work has been performed to establish realistic safe vibration criteria for pipelines in the vicinity of rock blasting in a variety of blasting situations (Siskind, et al, 1994).

### **3.1 Allowable Stress in Pipelines**

Generally, safe blasting criteria for transmission pipelines are specified by industry in terms of a maximum allowable stress. Circumferential or hoop (as opposed to longitudinal) stresses are usually used as these correspond to the critical state of operating stress. Hoop stresses produced by internal pressurization can be computed from the thin-walled cylinder equation:

$$\sigma = \frac{PD}{2t} \tag{6}$$

where, P is the actual operating pressure, 400 psi, D is the pipe inside diameter of 19.75 in and 11.75 in for the two pipelines, and t is the wall thickness, 0.25 in

The maximum hoop stress for both X-42 and X-52 pipelines of a constant diameter is assumed to be the same, because both pipelines have the same wall thickness and diameters, and operate at the same operating pressure. The maximum hoop stresses calculated for 20 in and 12 in diameter pipelines are 15,800 psi and 9400 psi, respectively.

It is general industry practice by some transmission companies to use 18% of the specified minimum yield strength (SMYS) as a limit to transient loads imposed on pipelines (Siskind, et al., 1994). This informal guideline takes into effect environmental and transient loads such as traffic over a pipeline beneath a highway. As such, 18% of the SMYS for the X-42 and X-52 steel pipe are:

$$X-42 \quad 0.18 * 42,000 \text{ psi} = 7560 \text{ psi}$$

$$X-52 \quad 0.18 * 52,000 \text{ psi} = 9360 \text{ psi}$$

For the X-42 pipe, this limit represents 47.8% and 80.4% of the circumferential stress produced by the actual operating pressure in the 20 in and 12 in diameter pipelines, respectively. For the X-52 pipe, this limit represents 59.2% and 99.6% of the circumferential stress produced by the actual operating pressure for the 20 in and 12 in pipelines, respectively.

Enron (1988) proposed other criteria which is used by the transmission industry and are judged to be highly restrictive. The Enron standard specifies an allowable stress of 1000 psi (6.9 MPa) for electrically welded and 500 psi (3.45 MPa) for gas-welded or mechanically jointed steel pipes.

The problem then becomes one of relating maximum allowable stresses to the stresses imposed in the pipeline from ground motion particle velocities resulting from blasting. It is most convenient to relate pipeline motions, in terms of strains and stresses in the pipeline than compare the stresses imposed by blasting to the maximum allowable stress for a specified grade of steel. However, this requires dynamic strain measurements using gages placed directly on the pipeline surfaces. Such measurements are difficult to

make, requiring removal of the cathodic protection, and instrumentation systems often cannot withstand the harsh environments presented during construction blasting operations. These measurements are better suited during a controlled research situation at great expense and over long time duration. It is convenient to use readily available ground motion instrumentation (e.g. blasting seismographs) to estimate strains and stresses in pipeline using elastic stress-strain relationships.

### **3.2 Blasting Vibration Criteria for Pipelines**

In 1994, the U.S. Bureau of Mines conducted an extensive study to measure buried pipeline response to surface coal mine blasting in southern Indiana (Siskind, et al., 1994). Five pressurized pipelines of various diameters, wall thicknesses, age, working pressures and material types were buried at distances ranging from 3500 ft to 5 ft away from the blasting. Strain gages and velocity sensors were placed on the pipeline. Ground motion velocity transducers were used to monitor the ground responses to blasting. The study took place over 6 months and included full-scale production blasts using 12.2 in diameter blastholes and charge weights of 4200 lbs per delay. For large blasts that did not produce permanent ground displacement near the pipelines, the highest pipeline velocity response was 10.8 ips with corresponding surface ground motions of 25.5 ips at a distance of 15 ft from the closest blasthole. Strains recorded on the steel pipeline for this largest blast were 94.8  $\mu$ -strains (circumferential) and 156  $\mu$ -strains (longitudinal). The PVC pipeline longitudinal strain was 499  $\mu$ -strains. It was found that at low vibration levels the circumferential or hoop strains were two times the longitudinal strains while at

higher vibration levels they were equal in magnitude. No pipe lost pressure or experienced failure at these high levels of velocity.

A procedure to determine safe ground motion velocities at the ground surface above pipelines to ensure pipeline stresses remained below the allowable stress is given from correlations made with circumferential or hoop (“worst case”) strains and radial and vertical components of ground motions (Aimone-Martin, 2001). The strain level associated with the minimum allowable stress (defined as 18% of the specified minimum yield strength of SMYS) was used to compute a corresponding peak particle velocity to be measured in the ground to ensure that pipeline strains remain below the 18% criteria.

Two useful relationships provided in the Siskind data report were empirically derived and are:

$$\varepsilon_c = 24.3 V \tag{7}$$

$$\varepsilon_c = 24.1 R \tag{8}$$

where,  $\varepsilon_c$  is the circumferential strain (in  $\mu$ -strain), V and R are the peak values of ground motions for the vertical and radial components in term of inches per second (ips). These linear relationships represent the upper envelope (or worst case line) that includes all measurements recorded in the field over six-month project duration for three grades of steel pipe (Grad B, X-42 and X-56).

Unfortunately, the U.S. Bureau of Mines research failed to encourage vibration limits set at realistic levels in the U.S. Limitations on blasthole charge weights near pipelines continue to be conservative and are not consistent from state to state or among pipeline transmission companies. As such, there are no current uniform mining industry

guidelines for blasting near gas transmission pipelines. Table 3.1 summarizes representative samples of guidelines or regulations existing in coal mining states (Aimone-Martin, 2001). Generally, vibration limits are set based on the measured maximum peak particle velocity (PPV in ips) or based on the shot-to-pipeline distance. Table 3.1 indicates that each state surveyed is unique in the approach to setting limits.

Table 3.1 Summary of vibration limits imposed in representative coal mining states<sup>(1)</sup>

<b>State</b>	<b>Distance limit (ft)</b>	<b>Peak Particle Velocity Limits (ips)</b>	<b>Frequency Limits (Hz)</b>	<b>Comments</b>
Illinois	100	None	None	(1) seismograph monitoring
Indiana	None <sup>(1)</sup>	4.0	None	is required within 500 ft
Kentucky	None	2.0 – 4.0	None	Blaster and pipeline owner must agree to other limits
Ohio	50 (quarries) 300 (surface mines)	None	None	Variance can be obtained for distance limits Blaster and pipeline owner
Pennsylvania	None	None	None	must agree on a peak ground velocity limit Generally, the closest
Virginia	None	4.0 – 5.0 set by mine permit	None	distance is 2 times the borehole depth

(1) Information obtained by surveying the state regulatory agency responsible for explosives use and safety

### 3.3 Procedures to Estimate Strains and Stresses in Pipeline from Velocity Measurements

The biaxial stress-strain relationships, shown on the pipeline schematic in Figure 3.2, are given by the following:

$$\sigma_c = \frac{E}{(1-\nu^2)}(\varepsilon_c + \nu\varepsilon_l) \quad (9)$$

$$\sigma_l = \frac{E}{(1-\nu^2)}(\varepsilon_l + \nu\varepsilon_c) \quad (10)$$

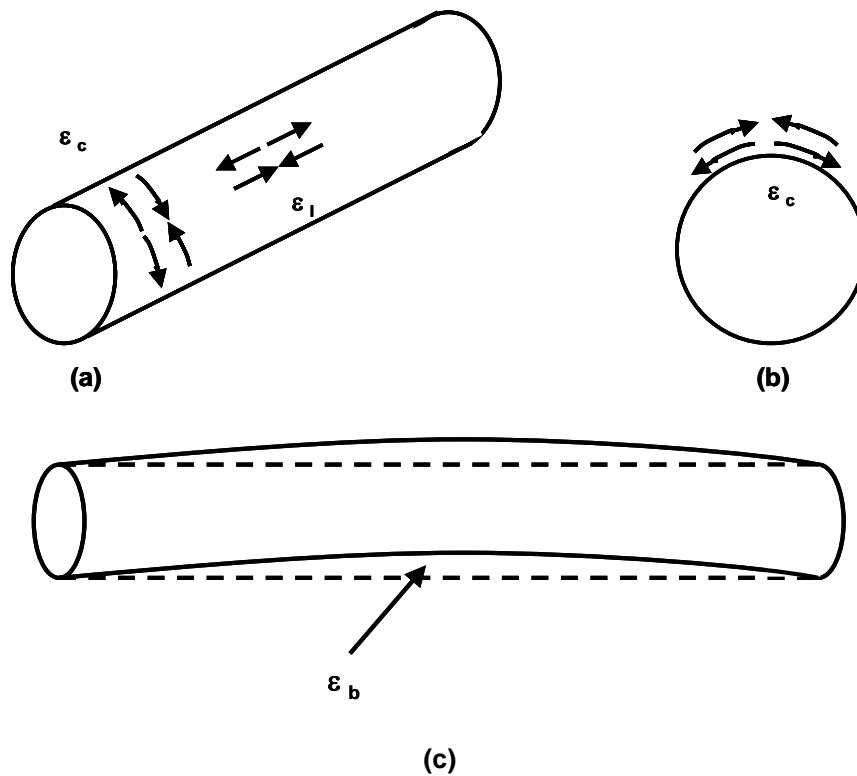


Figure 3.2 (a) Longitudinal,  $\varepsilon_l$  and (b) circumferential,  $\varepsilon_c$ , and (c) bending,  $\varepsilon_b$ , strain components of pipeline deformations

where,  $\sigma_c$  is the circumferential or hoop stress;  $\sigma_l$  is the longitudinal stress,  $\varepsilon_c$  is the circumferential strain,  $\varepsilon_l$  is the longitudinal strain, E is the Young's modulus of elasticity, and  $\nu$  is the Poisson's ratio. Bending stress is given by

$$\sigma_b = E\varepsilon_b \quad (11)$$

Gages mounted on a pipeline to record strains in the longitudinal and circumferential directions can be used to measure the strains directly. Knowing the elastic properties of the steel pipeline, the stresses induced in the pipeline can be easily computed. The time and expense to use strain gages is not always justified for many short-term projects. Thus, when strains cannot be directly measured, they can be estimated from peak velocity measurements. In this case, the response of pipelines to blasting vibrations is limited to pipe bending and stretching (or longitudinal strain) where:

$$\varepsilon_b = \frac{Vr2\pi f}{C_s^2} \quad (12)$$

$$\varepsilon_l = \frac{V}{C_l} \quad (13)$$

where,  $\varepsilon_b$  is the bending strain,  $\varepsilon_l$  the longitudinal strain, V is the maximum peak velocity measured on the pipeline for the corresponding component,  $C_s$  is the shear wave velocity,

$C_1$  the compressive wave velocity,  $f$  is the frequency of the velocity time histories at the peak  $V$ , and  $r$  is the radius of the pipeline.

When the direction of the incoming ground motion from blasting is perpendicular to the long axis of the pipeline,  $V$  in Equations (12) and (13) becomes  $R$  and  $T$ , respectively.

Circumferential or hoop strains can be estimated from the shear strain,

$$\gamma = \frac{V}{C_s} \sim \varepsilon_c \quad (14)$$

The above analysis is valid assuming that the pipeline is sufficiently flexible and deforms with the ground surrounding the pipe. Newmark and Hendron (Peck et al., 1972) defines the flexibility ratio,  $J$ , as:

$$J = \frac{E/(1+\nu)}{\left[ \frac{6E_p I_p}{(1-\nu_p^2)} \right] \left( \frac{1}{r^3} \right)} \quad (15)$$

where,  $I_p$  is the moment of inertia of the pipe,  $\left( \frac{1}{12}(r^3 b) \right)$ ,  $t$  is the pipe wall thickness, and  $b$  is a unit length along the pipe axis.

The subscript “P” refers to the pipeline properties while the constants without subscripts refer to the properties of the surrounding soil (backfill) media. If  $J > 10$ , the buried pipeline has a low stiffness compared to the confining media and the elastic formulas given above apply.

For the pipelines used in this study, it is assumed that the sandy soil backfill has the following properties:

$$E = 20,000 \text{ psi}$$

$$\nu = 0.25$$

Given the elastic properties and dimensions for the pipe,  $J$  is calculated as 63.5 and 13.72 for the 20 in and 12 in pipeline, respectively. Thus, the elastic equations can be used to estimate strain from velocity measurements for these pipelines.

## 4 INSTRUMENTATION

### 4.1 Structure Vibrations

Figure 4.1 shows a plan view of the instrumentation locations within, and exterior to, the Unser road residence used in this study. The location of the interior, single component velocity transducers placed in the upper (S2) and lower (S1) corners, and on the mid-walls in the living room are indicated in Figure 4.2. LARCOR<sup>TM</sup> multi-component seismographs were used to digitally record four channels of seismic data. The exterior (master) unit consisted of a tri-axial geophone and an airblast microphone. The tri-axial geophone was buried at a depth of 6 in, and oriented so that the radial, R, and transverse, T, components were perpendicular and parallel respectively to the east wall containing the instrumented crack. This orientation is based upon recording motions that are parallel to one of the house's translation axes rather than the traditional direction relative to the vibration source. The airblast microphone was installed at a height of 18 in above the ground surface and was used to record the pressure pulses transmitted through the air during blasting.

Both the S1 and S2 seismographs were connected to clusters of three single axis transducers in the upper and lower interior corners and adjoined mid-walls (north or east wall) as shown in Figure 4.2. These transducers were affixed to the walls using hot glue to minimize damage during removal. The three corner transducers, labeled R, T, and V in Figure 4.3(a) and 4.3(b), measure whole structure motions in the radial, transverse (horizontal), and vertical directions, respectively, for the upper and lower corners. The mid-wall transducers measured horizontal motions during wall flexure or bending.

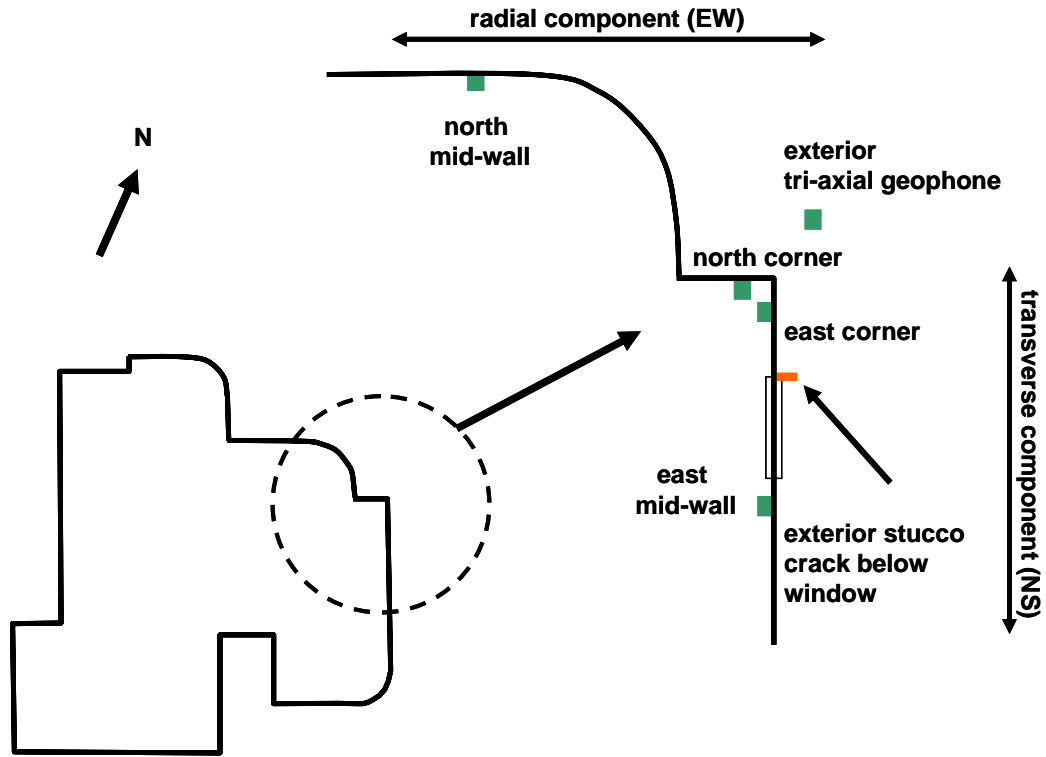


Figure 4.1 Schematic plan view of the resident showing the location of the single velocity component transducers and the crack gauge



Figure 4.2 Location of velocity transducers to measure structure response in the walls

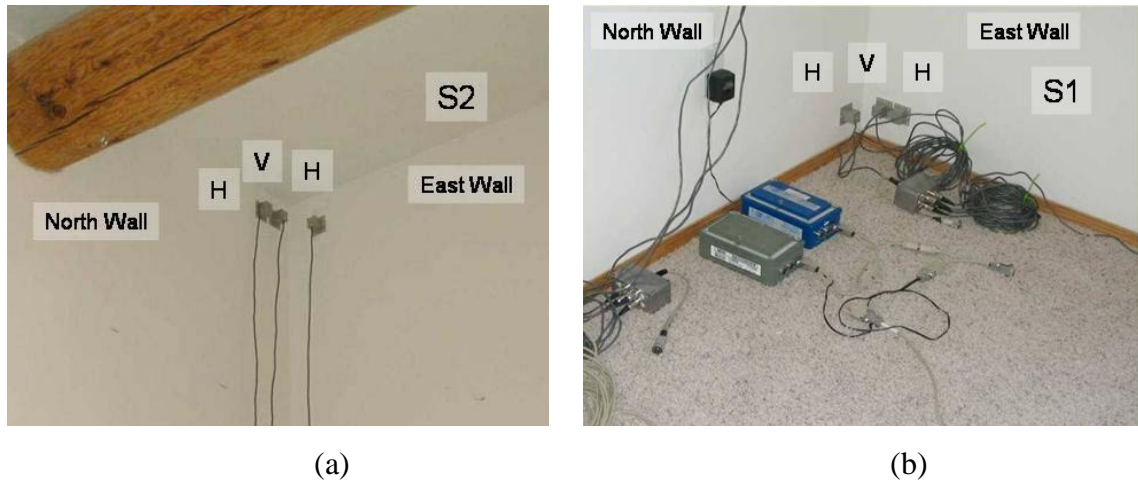


Figure 4.3 Details of velocity transducers locations in the (a) upper (S2) and (b) lower (S1) corner

The three seismographs used were connected in series, with the exterior serving as the master (triggering) unit, and the interior as slave units, as showed in Figure 2.1. The master unit activated automatically when a ground particle velocity or airblast is greater than the pre-set trigger levels was detected. Upon triggering, the master unit delivered a +1 volt pulse to the slave units via the serial cable. The slave units were set in the manual mode activated and began recording data upon receiving the +1 volt pulse. The master and slave units recorded with a common time base. Thus, the seismograph records are time-correlated, which is critical for later analysis.

The master and slave seismographs each had a range of available setting for recording data. These settings include:

- Trigger levels for the master unit set to 0.03 inches per second (ips) for ground particle velocity, and 130 decibels (dB) for airblast;
- Sample rate set at 512 samples per second;
- Sampling duration between 9 and 18 seconds.

These settings ensured the full data record was preserved in sufficient resolution.

## **4.2 Crack Displacements**

To measure the effect of blasting and climate conditions (temperature and humidity) on changes in the width of existing exterior cracks, Kaman™ eddy-current gages were installed, as shown in Figures 4.4 and 4.5, and data was collected using a SOMAT™ field computer. A schematic of the data acquisition system is given in Figure 4.6. Each Kaman gage consisted of mounting brackets, one of which served as a target plate, and an active element. Gages were mounted in brackets affixed to the stucco exterior wall over an existing crack (crack gage) and on an un-cracked surface (null gage) on the structure. The crack gage was installed with each mounting bracket placed on either side of the crack. One bracket held the active element against the target plate (second bracket) at a sufficient gap distance to allow the gage to function properly.

Operation of eddy-current gages relies on the property of electrical induction. The sensor consists of a coil of wire driven by a high frequency current that generates a magnetic field around the coil. If a non-magnetic conductive target material is introduced into the coil field, eddy-currents are induced in the surface of the target material. These currents generate a secondary magnetic field in the target, inducing a secondary voltage in the sensor coil (active element), resulting in a decrease in the inductive reactance in the coil. This type of system is also known as variable impedance because of the significance of the impedance variations in defining its complex nature (Hitz and Welsby, 1997).



Figure 4.4 Location of Kaman gages and SOMAT field computer on the east wall of the structure



Figure 4.5 Close up in the gage active element (left) and brackets mounted in an existing crack (right)

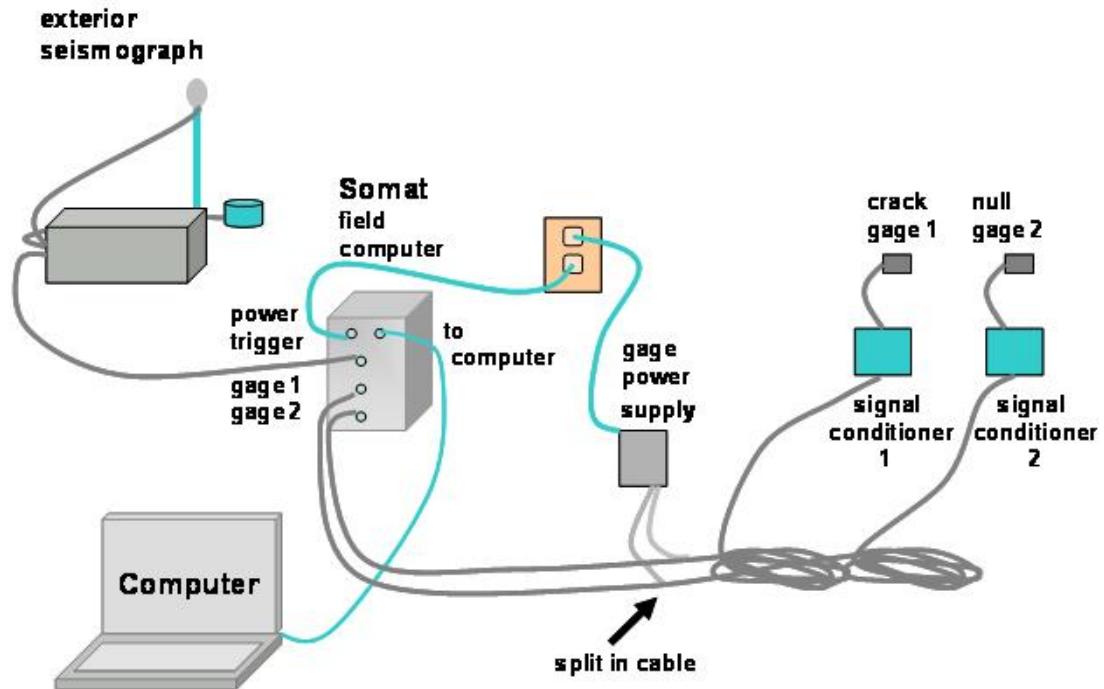


Figure 4.6 Displacement gage system used to measure opening and closing of an existing crack

The Kaman gage system was programmed to sample crack opening and closing every hour in response to diurnal environmental changes. In the dynamic or ‘burst’ mode, data was acquired every 0.001 seconds. Temperature and relative humidity were recorded using a SUPCO™ data logger. A sample interval of 10 minutes was used.

The operating parameters of the Kaman gages are as follows:

- Displacement monitoring range of 0.02 inches.
- Output voltage range  $\pm 5$  volts.
- Resolution of 3.94 micro-inches. (.00000394 in)
- Frequency response of 10,000 Hertz (Hz).

### **4.3 Pipeline Response**

The instrumentation of the pipelines (SE and NW pipelines) at study site took place on September 21, 2004. The response of the pipelines and surround ground was measured for 9 construction blasts (trench and road blasts) between September 21 and October 28, 2004, using single axis velocity transducers and blasting seismographs.

#### **4.3.1 Instrumentation Design and Implementation**

On September 21, 2004, sections of the 20 in and 12 in pipelines were excavated, one in the SE part of the site (X-42 pipelines), and another in the NW part of the site (X-52 pipelines), for the purpose of placing instruments on the pipelines. The placement of the velocity sensors on the pipelines is shown in Figure 4.7. Three single component velocity transducers were mounted on the pipeline using epoxy to record velocity in the R, T, and V directions. As shown in Figure 4.8, the V and T sensors were placed at the top of the pipeline while the radial component, R, was placed at the side of the pipeline, oriented toward the blast. The pipelines were not covered with fill during blasting studies and left exposed. The fact that the pipelines were not confined may have influenced the vibrations measured directly on the pipelines in the vertical direction. It is assumed that the exposed pipe section was sufficiently short such that the R and T components presented fully buried pipes.

Tri-axial geophones were buried in the ground 6 in at the ground surface above the pipelines, in the middle of the distance between the pipelines. All velocity transducers were 2 Hz vibration sensors manufactured by Mark Products or Geospace and assembled by LARCOR, of Dallas, TX.

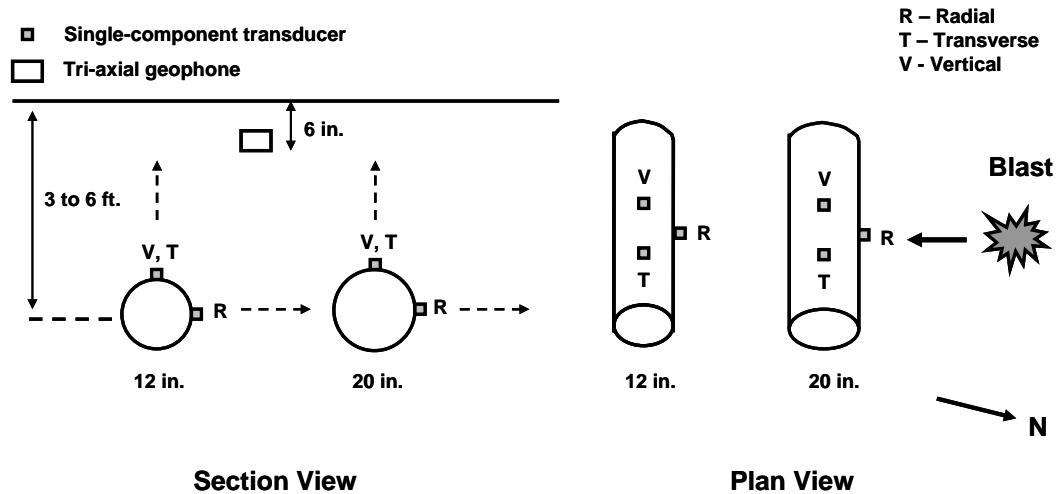


Figure 4.7 Section (looking west) and plan views showing the location of the velocity sensors on the pipelines

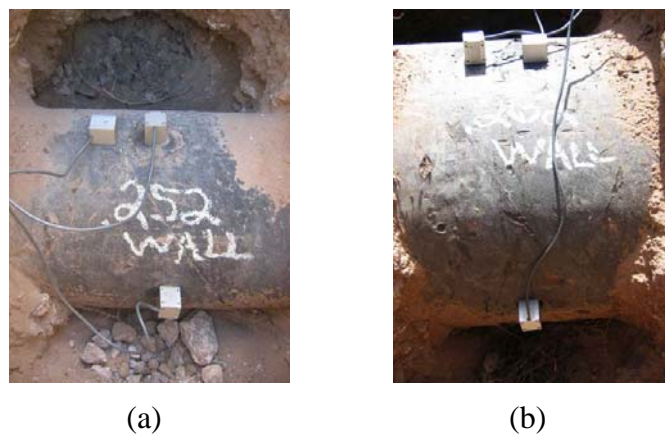


Figure 4.8 Attached single component transducers to the pipeline top, components V and T and to the side facing the blast, component R, for (a) 12 in X-42 pipeline and (b) 20 in X-42 pipeline

The transducers and the airblast microphone were connected to three blasting seismographs that were connected together in series. The geophone buried at the ground surface and the airblast microphone were connected to the master seismograph used to trigger the system on a pre-selected ground motion level. The single-component transducers, on both pipelines, were connected to two “slave” seismographs. Upon

triggering, the master unit sent a +1 volt spike to the slave units to start the data recording process for all three seismographs at the same time. In this manner, each seismograph recorded velocity data simultaneously on one common time base.

All three seismographs were programmed to record 12 seconds of record time at a sample rate of 512 samples per second. The master unit was set to trigger at a ground motion of 0.03 ips and the maximum range varied from 2.5 to 5.0 ips, depending on distance and pounds per delay of the blast holes.

#### **4.4 Data Acquisition and Reduction**

Full waveform time histories were digitally recorded and stored for each blast in the LARCOR<sup>TM</sup> multi-component seismographs. The data was downloaded from the seismograph units and analyzed using the White<sup>®</sup> seismograph data analysis program. Fast Fourier Transform (FFT) analysis was performed to evaluate the frequency content of the waveforms.

Crack gage data were downloaded from the SOMAT<sup>TM</sup> field computer and analyzed using SOMAT WINTCS v.2.0.1 and SOMAT<sup>TM</sup> DataXplorer v. 3 softwares. Crack displacement time histories were filtered using Data Filter, (Mercer, 2002) a spectrum filtering program to remove system noise and enhance the data signal-to-noise ratio.

## 5 CONSTRUCTION BLAST DESIGNS

### 5.1 Blasting Patterns

In this project, two types of blast designs were used and included road cut blasting extending Unser Road and trench cut blasting to install utility lines shown in Figure 5.1. Table 5.1 summarizes the construction blast designs used in the project. The distance is defined as the distance from the house or pipeline to the closest blast hole in the shot pattern. The maximum charge weight detonated within any 8 millisecond delay is specified. Blast holes were typically spaced in a rectangular pattern or in a single row (pre-split). The explosive charges used were 100% ammonium nitrate and fuel oil (ANFO).

The standoff distances varied from 758.5 ft to 1208 ft to the house and 57 ft to 201 ft to the pipelines. Scaled distance factors ranged from 8.8 to 75.2 ft/lb<sup>1/2</sup> for the pipelines and 65.5 to 560.0 ft/lb<sup>1/2</sup> for the house. The blasting grid patterns, burden and spacing, ranged from 4 by 5 feet to 5 by 5 feet with surface delays varying from 17 ms to 25 ms. The borehole diameter was 3 inches and the drill depths ranged from 4 to 21 feet. Usually each blast was covered with 3 to 5 feet of soil to avoid fly rocks, as shown in Figure 5.2.



Figure 5.1 Construction blast designs, road cut (left) and utility trench (right)

Table 5.1 Summary of blast designs used during the response study (PPV on the ground)

Shot Type	Shot Date	Structure	Distance from Structure (ft)	Charge Weight/Delay (lb)	Scaled Distance (ft/lb <sup>1/2</sup> )	Peak Particle Velocity (in/sec)	Frequency at the PPV (Hz)	Airblast (dB)	Number of holes
trench	09/16/04	house	970	5	433.8	0.035	8.5	100	78
trench	09/17/04	house	970	3	560.0	0.04	14.6	112	86
road cut	09/21/04	house	1208	25	241.6	0.135	6.6	110	320
		pipeline	110	25	22.0	1.96	4.3	124	
trench	09/23/04 a	house	980	7.5	357.8	0.045	14.2	100	300
		pipeline	206	7.5	75.2	0.15	17	112	
trench	09/23/04 b	pipeline	161	5	72.0	0.13	21.3	116	60
road cut	09/30/04	house	950	18.5	220.9	0.125	7.3	112	290
		pipeline	165	18.5	38.4	0.84	6.2	123	290
trench	10/07/04 a	pipeline	160	10	50.6	0.1	32	116	200
road cut/PS	10/07/04 b	pipeline	116	48	16.7	1.66	11.6	140	162/97 PS
road cut	10/14/04 a	pipeline	57	41.5	8.8	5.08	19.6	129	103
trench	10/14/04 b	pipeline	136	10	43.0	0.2	36.5	118	20
trench	10/28/04	pipeline	85	10	26.9	0.68	23.2	116	48
road cut	12/15/04	house	1137	110	108.4	0.175	4.4	112	256
road cut/PS	12/30/04 a	house	962	216	65.5	0.365	5.2	117	311/109 PS
road cut	12/30/04 b	house	962	40	152.1	0.125	4.5	110	48
road cut/PS	01/07/05	pipeline	91	80	10.2	5.6	12.1	124	81/15 PS
road cut	01/12/05	pipeline	83	39	13.3	2.8	17	124	36
trench	01/12/05	pipeline	180	22.5	37.9	0.42	10.6	118	108
trench	01/27/05 a	house	758.6	32	134.1	0.155	18.2	106	154
trench	01/27/05 b	house	758.6	32	134.1	0.055	9.8	nd	42
trench	01/28/05	house	1031.8	50	145.9	0.145	10.2	120	103

PS – pre-split



Figure 5.2 Trench blast been covered with sand

## 5.2 Wave Propagation Velocity Measurement

A series of seismographs were placed in a linear array during a road blast on September 21 to determine the wave propagation velocity through the ground. Figure 5.3 shows the layout of the seismographs, starting from the closest blasthole, passing through the pipelines and ending near the house. Each seismograph unit was connected in series to record the time history of ground motion on a common time base. The linear array of distances ranged from 13 ft to 290 ft from the closest blasthole. The arrival times of the first pulse at each geophone locations was used to compute the velocity of the ground motion between each two adjacent recording units. The vertical (V) component was used to establish the compressional sound speed in the rock and the transverse (T) component is assumed to approximate the shear wave velocity. The graph in Figure 5.4 shows the data plotted for each component and the slope of the line gives the wave speed. The

compressive wave speed ( $C_l$ ) was computed as 1620 ft/s, and the shear wave velocity ( $C_s$ ) is computed as 996 ft/s, approximately 61% of the compressive velocity.

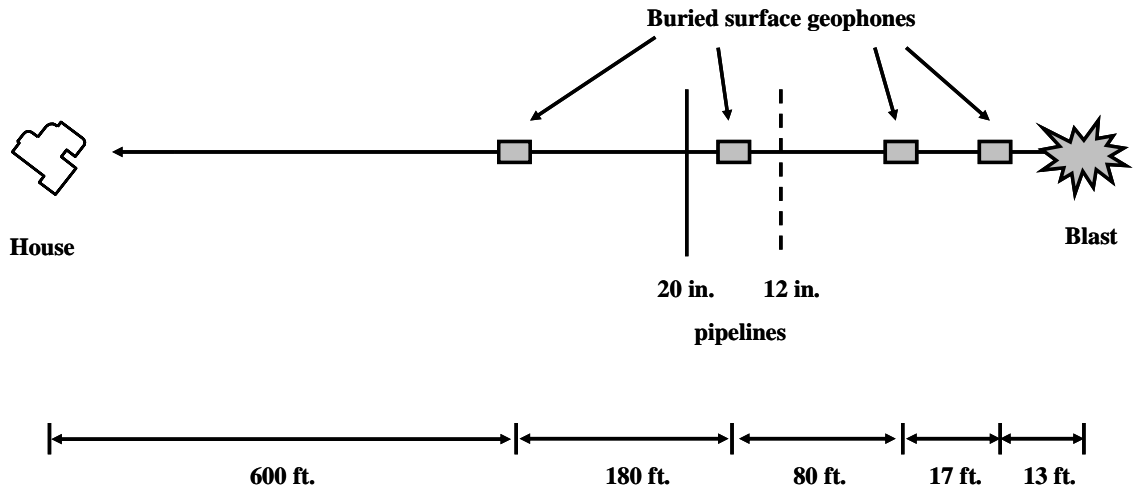


Figure 5.3 Seismograph array used to measure wave speed velocity in the ground

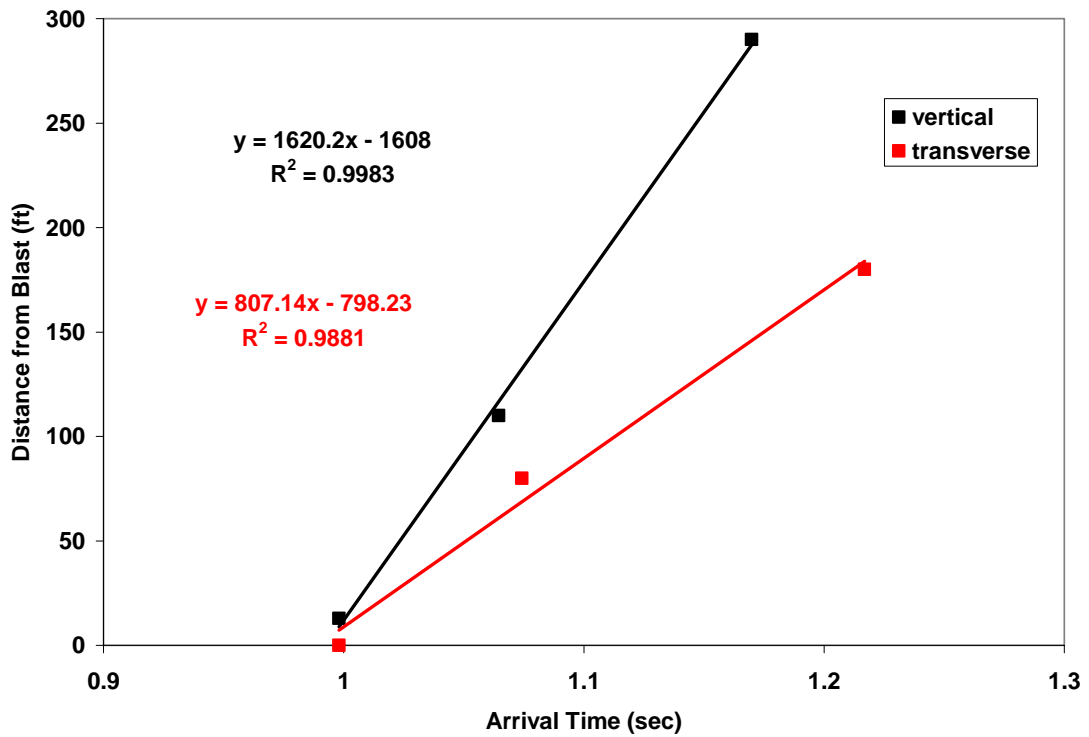


Figure 5.4 Wave speed in the ground

## 6 RESULTS

The results of this study are given in three sections. The first section summarizes the ground velocities and airblasts for all blasts conducted during the attenuation study. The second section presents the whole structure and mid-wall responses to dynamic events, and the crack responses to both transient (dynamic) structure motions and static, long-term environmental changes. Wall strains are computed in this section. The third section presents the pipeline response to dynamic events.

Seismograph reports are given in Appendices A through C. Appendix D contains summary table of all velocity and airblast values for the various seismographs. Data are given by blast date and include location of the seismograph, distance to the closest blasthole, charge weight per 8 ms delay, maximum peak velocity values and frequencies, and airblast measured for each seismograph. Appendix E present maps of instrumented structure locations and outline of the blasting pattern.

### 6.1 Ground Motion and Airblast Characteristics

Figures 6.1 and 6.2 are plots of scaled distance factor versus peak ground motions and airblast, respectively. The attenuation study included very close-in measurements (up to 5 ft from the blasts) to better define attenuation slopes taking into account both distance from the blast and the explosive charge weights used in design. Scaled distance factors are applied to ground motions and airblast, given by the following:

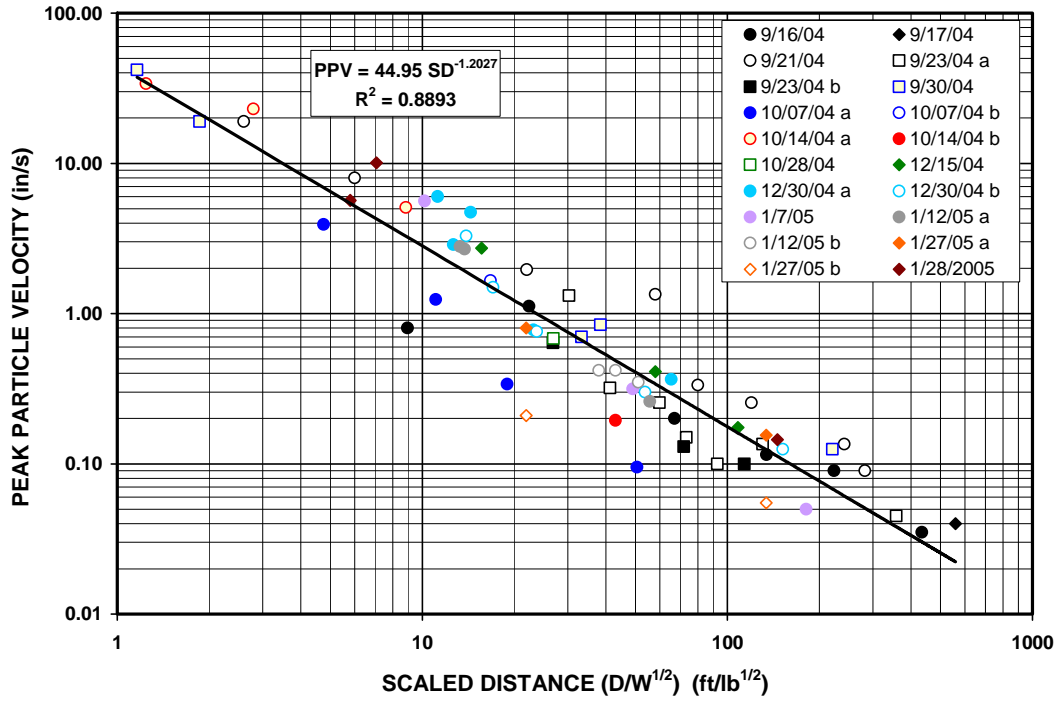


Figure 6.1 Peak particle velocity in the ground versus scaled distance for the attenuation study, the data is divided by date of the blast

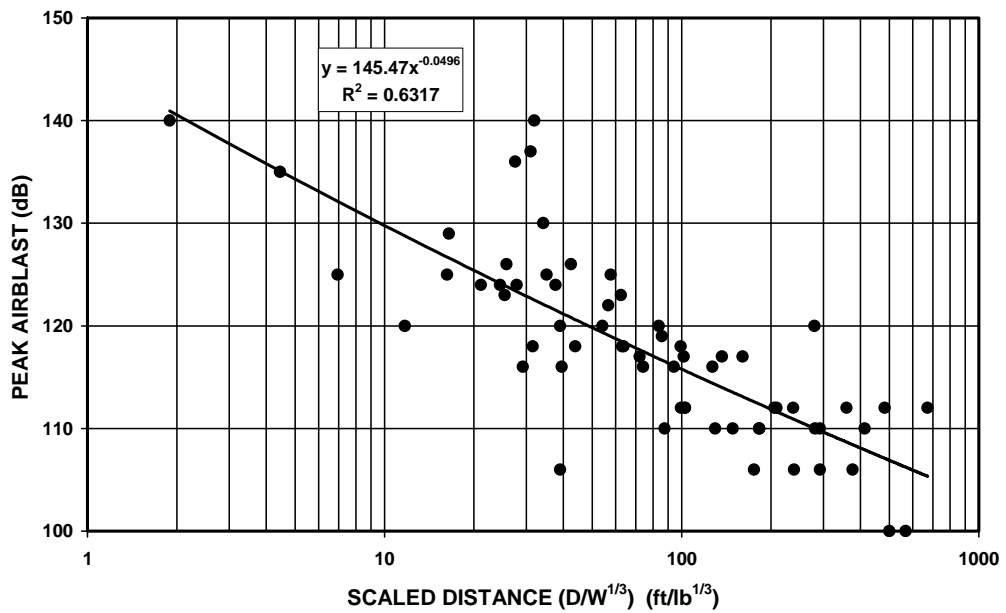


Figure 6.2 Peak airblast versus cube-root scaled distance for the attenuation study

Square-root scaled distance used to plot ground motions

$$SRSD = \frac{D}{W^{1/2}} \quad (16)$$

Cube-root scaled distance used to plot airblast

$$CRSD = \frac{D}{W^{1/3}} \quad (17)$$

where, D is the distance of the seismograph to the closest hole in the blast, and W is the maximum charge weight detonated within any 8 ms time period (referred to as one delay time period).

Scaled distance is a means of incorporating the two most important factors contributing to the intensity of ground motion and airblast, as intensity decreases proportionally with distance and inversely with the explosive weight detonated on one time delay. In the case of ground motion, the SRSD is used (commonly referred to as simply SD), as ground motion has been shown to correlate with the square root of the charge weight. In the case of airblast, air pressures correlate best with the cube-root of the charge weight, so the CRSD is used.

Attenuation plots are usually used to analyze the vibration data. The best-fit line through the data, shown in the plots, is a power curve of the form:

$$V = K * SD^{-b} \quad (18)$$

where

$K$  = the y-intercept at  $SD = 1$

$b$  = slope of the attenuation line

The  $K$ -factor measures the intensity of the seismic energy that is transferred into the ground and is propagated away from the blast site. It is a function of confinement, explosive density, and energy. The slope term, “ $b$ ” is related to the geology through which the seismic wave passes and is a measure of the decay of the velocity intensity with distance.

## **6.2 Structure Response to Blasting**

Seismograph reports for the structure response for all blasting events are given in Appendix B. Appendix F contains a summary table of all velocity and airblast values for the seismographs placed in the house. The data are given by blast date and includes peak velocity values and frequencies for the three components of ground motion and for the single component interior geophones, upper (S2) and lower (S1) corners.

Table 6.1 summarizes the blasting data and the peak particle velocity and airblast recorded by the ground motion geophone at the structure. This table contains the blast dates, the distance from the blast to the structure, the charge weight per 8 ms delay, and the peak ground motion, frequency, and airblast. Tables 6.2 and 6.3 summarize the data of structure response for the east and north walls, respectively. It contains the peak particle velocity recorded by the sensor in each wall and compares this data to the ground motion and airblast for similar components.

Table 6.1 Summary of blasting data, ground motion and airblast in the structure

Shot Date	Distance From Structure (in)	Charge Weight/Delay (lb)	Scaled Distance (ft/lb <sup>1/2</sup> )	Peak Particle Velocity (in/sec)	Peak Frequency (Hz)	FFT Frequency (Hz)	Airblast (psi)
9/16/2004	970	5.00	433.8	0.035	8.5	8.94	0.0003
9/17/2004	970	3.00	560.0	0.040	14.6	7.94	0.0012
9/21/2004	1208	25.00	241.6	0.125	3.7	4.31	0.0009
9/23/2004	980	7.50	357.8	0.045	14.2	7.88	0.0003
09/30/04	950	18.50	220.9	0.12	7.7	5.56	0.0012
12/15/04	1137	110.00	108.4	0.175	4.4	4	0.0012
12/30/04a	962	216.00	65.5	0.365	5.2	3.25	0.002
12/30/04b	962	40.00	152.1	0.125	4.5	3.25	0.0009
1/27/05a	758.6	32.00	134.1	0.155	18.2	12.25	0.0006
1/27/05b	758.6	32.00	134.1	0.055	9.8	8.38	nd
1/28/2005	1031.8	50.00	145.9	0.145	10.2	5.88	0.0029

nd – no data

### 6.2.1 Comparison of Structure Response with Ground Motions and Airblast

It is often useful to visually compare the response of a structure (upper and lower corners and mid-wall) with ground motion and airblast excitations that induce structure motions. Representative velocity time histories for the blasts generating the greatest dynamic crack response were selected for the structure and are illustrated in Figures 6.3 and 6.4. The blasts dates are 12/30/04, first blast, and 01/27/05, first blast, as two blasts were conducted in those days.

Figures 6.3 (a) and (b) and 6.4 (a) and (b) show time histories comparing the ground motions and airblast with structure motions. The lower corners (S1) for the structure compare closely with the ground velocities (GV) for the two horizontal components (T, transverse, and R, radial, shown as north and east walls, respectively), indicating good coupling of the structures with the foundations, as can be seen in the first row of the figures.

Table 6.2 Summary of structure response for the east wall

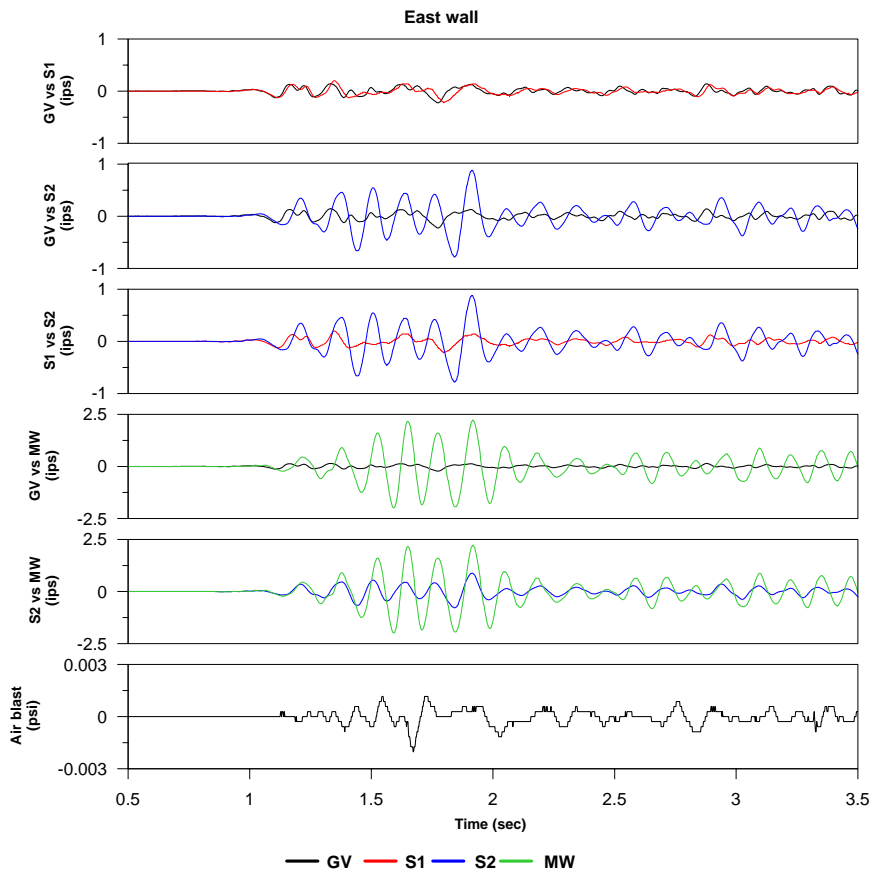
Shot Date	GROUND MOTION AND AIRBLAST				S1- WALL BASE			S2- WALL TOP			EAST MID-WALL		
	Radial Peak Velocity	Peak Frequency	FFT Frequency	Airblast	Peak Corner Velocity	Peak Frequency	FFT Frequency	Peak Corner Velocity	Peak Frequency	FFT Frequency	Peak Wall Velocity	Peak Frequency	FFT Frequency
	(in/sec)	(Hz)	(Hz)	(psi)	(in/sec)	(Hz)	(Hz)	(in/sec)	(Hz)	(Hz)	(in/sec)	(Hz)	(Hz)
09/16/04	0.025	8.5	8.94	0.0003	0.025	15.0	9.12	0.095	9.6	7.69	0.295	8.9	7.69
09/17/04	0.020	14.6	7.94	0.0012	0.025	15.0	7.31	0.105	8.3	8.06	0.325	8.3	8.06
09/21/04	0.125	3.7	4.31	0.0009	0.120	6.3	4.38	0.340	7.3	7.81	0.740	8.0	7.81
09/23/04	0.035	14.2	7.88	0.0003	0.030	11.6	7.62	0.200	8.5	7.94	0.475	8.2	7.94
09/30/04	0.120	7.7	5.56	0.0012	0.100	6.7	5.38	0.500	7.1	7.44	1.120	7.1	7.44
12/15/04	0.160	4.4	4.00	0.0012	0.150	4.1	4.06	0.440	6.5	7.81	0.860	6.7	7.81
12/30/04 a	0.225	5.2	3.25	0.0020	0.220	5.2	3.19	0.880	6.5	7.62	2.220	6.9	7.69
12/30/04 b	0.090	4.5	3.25	0.0009	0.095	6.4	6.38	0.415	6.9	7.75	0.880	7.3	7.85
01/27/05a	0.140	18.2	12.25	0.0006	0.100	11.6	9.15	0.400	8.2	8.00	1.040	7.5	8.00
01/27/05b	0.055	9.8	8.38	nd	0.035	9.8	9.50	0.125	8.5	8.12	0.350	9.1	8.12
01/28/05	0.145	10.2	5.88	0.0029	0.115	5.8	5.88	0.440	7.3	5.94	1.180	8.2	8.00

nd = no data

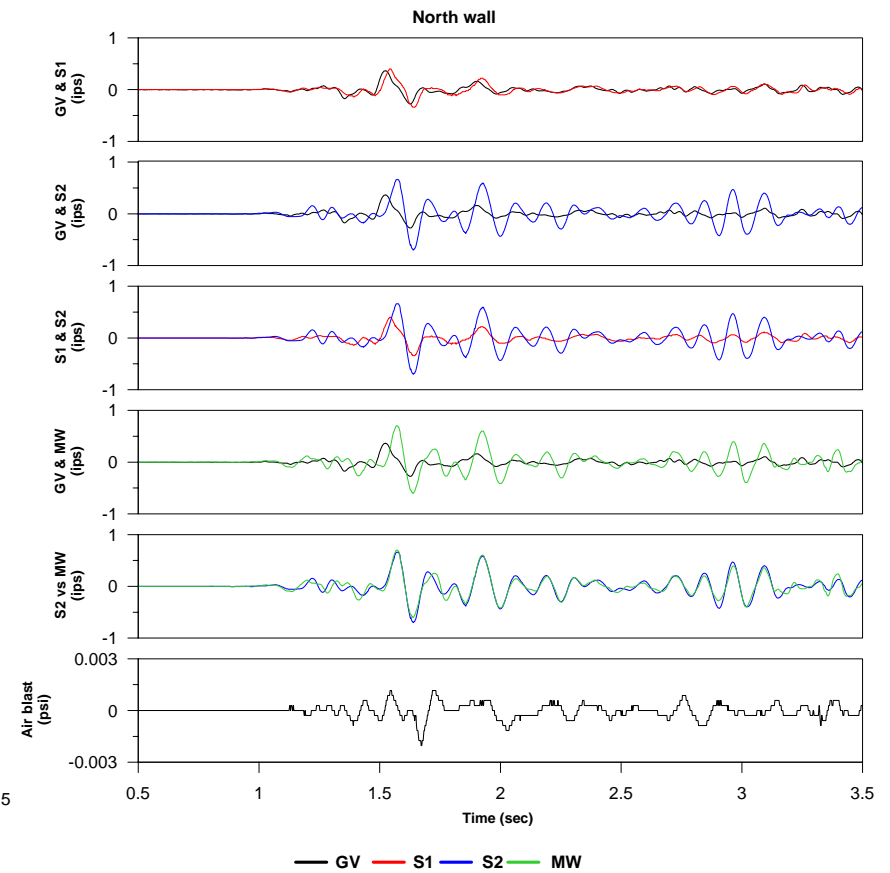
Table 6.3 Summary of structure response for the north wall

Shot Date	GROUND MOTION AND AIRBLAST				S1- WALL BASE			S2- WALL TOP			NORTH MID-WALL		
	Transverse Peak Velocity	Peak Frequency	FFT Frequency	Airblast	Peak Corner Velocity	Peak Frequency	FFT Frequency	Peak Corner Velocity	Peak Frequency	FFT Frequency	Peak Wall Velocity	Peak Frequency	FFT Frequency
	(in/sec)	(Hz)	(Hz)	(psi)	(in/sec)	(Hz)	(Hz)	(in/sec)	(Hz)	(Hz)	(in/sec)	(Hz)	(Hz)
09/16/04	0.035	8.5	8.94	0.0003	0.035	11.6	9.00	0.165	9.1	9.44	0.165	9.6	9.44
09/17/04	0.040	14.6	7.94	0.0012	0.030	10.0	8.00	0.120	9.3	10.25	0.110	9.6	10.25
09/21/04	0.095	3.7	4.31	0.0009	0.115	4.9	4.06	0.245	7.8	8.19	0.260	7.4	4.06
09/23/04	0.045	14.2	7.88	0.0003	0.035	12.1	8.50	0.135	10.2	8.06	0.125	10.6	8.06
09/30/04	0.095	7.7	5.56	0.0012	0.115	6.0	5.31	0.320	6.9	5.31	0.355	7.5	5.31
12/15/04	0.175	4.4	4.00	0.0012	0.220	4.7	4.06	0.485	6.5	8.69	0.565	6.9	4.06
12/30/04 a	0.365	5.2	3.25	0.0020	0.400	5.2	5.00	0.700	6.9	7.75	0.700	6.4	7.75
12/30/04 b	0.125	4.5	3.25	0.0009	0.100	4.0	3.38	0.330	7.7	7.00	0.295	8.2	7.00
01/27/05 a	0.155	18.2	12.25	0.0006	0.115	11.6	8.06	0.440	8.8	9.25	0.395	8.5	9.25
01/27/05 b	0.035	9.8	8.38	nd	0.040	10.6	8.12	0.175	9.4	10.25	0.170	10.2	10.25
01/28/05	0.105	10.2	5.88	0.0029	0.100	4.9	4.31	0.305	7.5	9.69	0.280	6.9	5.94

nd = no data



(a)



(b)

Figure 6.3 Velocity time histories comparisons of (a) east and (b) north ground motion (GV), lower corner (S1), upper corner (S2), mid-walls (MW), and airblast for the structure, first blast at 12/30/04

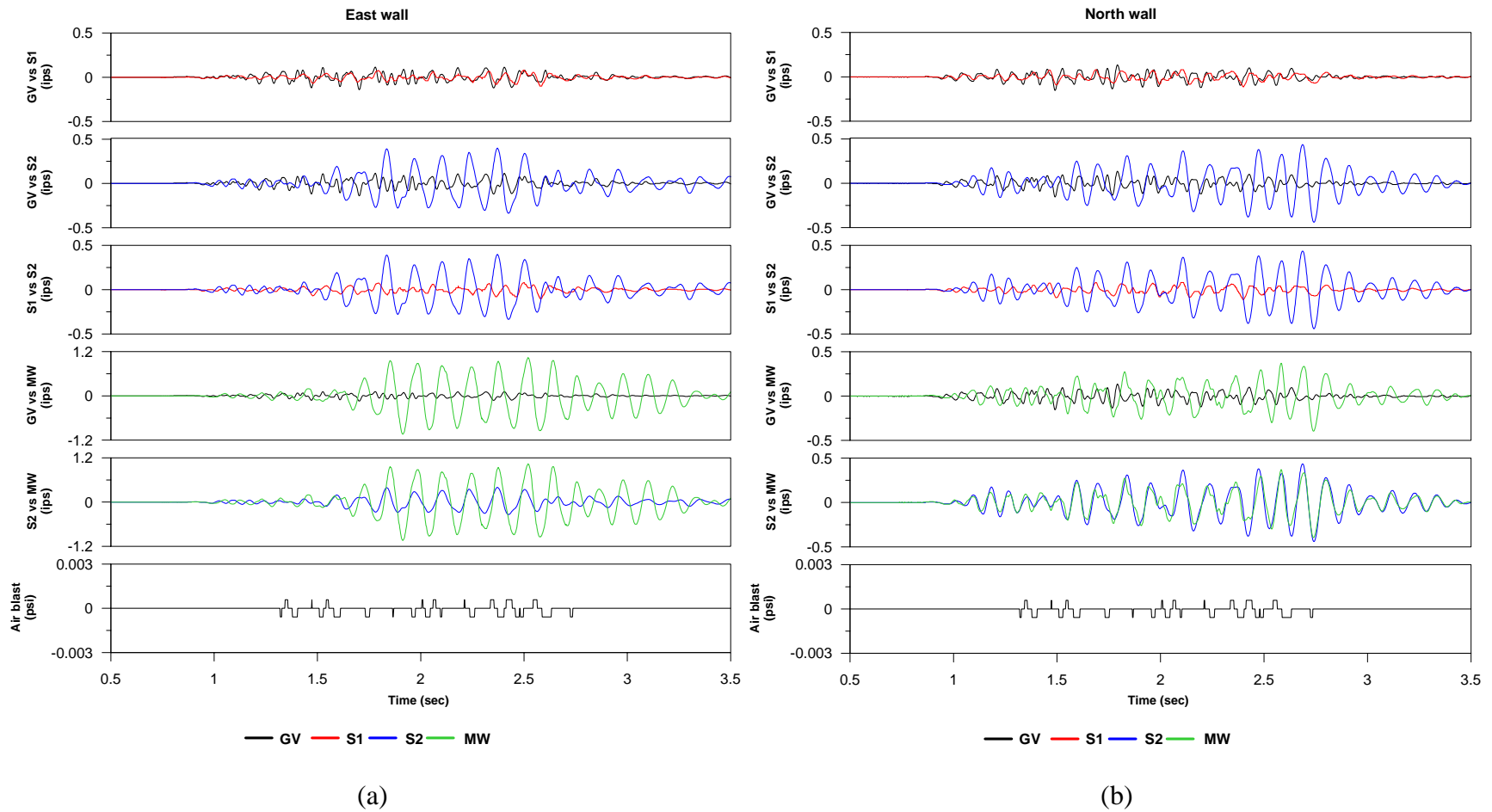


Figure 6.4 Velocity time histories comparisons of (a) east and (b) north ground motion (GV), lower corner (S1), upper corner (S2), mid-walls (MW), and airblast for the structure, first blast at 01/27/05

Row three in the figures compares the upper and lower corners motions and the waveforms show typical upper structure response relative to the lower structure with an significantly amplification of velocities in the upper structures. Amplification occurs because the upper walls are free to vibrate and are not well-coupled to the roof as the roof tended to move with the excitations. Another factor is that the walls at the leaving room in this structure are very high, with distance measured from lower corner to upper corner of 144 inches. The amplification in the upper structure can also be seen in the time histories of row two, which compare upper corner (S2) with ground motion (GV).

The influence of airblast is negligible and does not contribute to structure shaking, except for some cases, as for the blast at 12/30/04 (Figure 6.3) where it can be seen that the airblast has some influence in the increase of the mid-walls and upper (S2) motions. The frequency at the peak 117 dB airblast is 10.2 Hz which is close to the 9 Hz natural frequency of the structure (discussed below) and energy is not coupled within the walls at this low amplitude.

As illustrated in the fifth row of Figures 6.3(a) and 6.4(a), the mid-wall in the direction of the blasting respond with motions larger than the upper corners. The mid-wall tends to vibrate far greater than corners as corners are more restrained. Vibrations in mid-walls rarely lead to cracking but rather contribute to interior structure noise, as loose objects hanging on or leaning against walls tend to rattle with the wall motions. This rattling and resulting noise leaves persons inside a structure with the perception that structure damage is taking place. Mid-walls very often carry the same low frequencies and characteristic cycles (phases, or peaks and troughs) as the upper structure (S2), particularly later in the time histories when low frequencies persist. This is apparent in

the structures in the north wall, given in the fifth row of Figures 6.3(b) and 6.4(b). Time histories for the structure do not exhibit any unusual characteristics, and it responds as expected and within the range of structures of similar construction.

Figures 6.5 through 6.8 show correlations among structural components in response to ground motions (Figures 6.5 and 6.6) as well as the structural response to airblast pressure (Figures 6.7 and 6.8). Figure 6.5 shows the correlation between the upper structure (S2) peak velocity with the peak velocity recorded in the ground for similar components. The best fit coefficient,  $R^2$ , of the transverse component shows a 78% correlation compared with 86% for the radial component. This difference can be partially attributed to the fact that the GV tri-axial transducer and the radial component of S2 cluster are both on the east side of the structure and experience similar excitations. However, the transverse component of the S2 cluster is mounted on the north wall, and thus is somewhat less correlated to the transverse component of GV recorded on the east side of the structure.

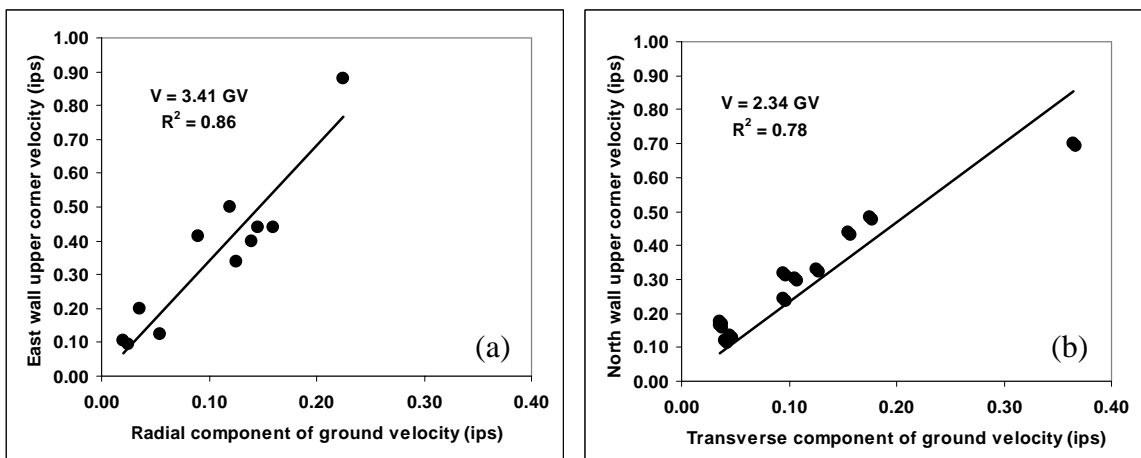


Figure 6.5 Ground velocity influence on peak motion of the upper structure corners for (a) radial and (b) transverse ground components

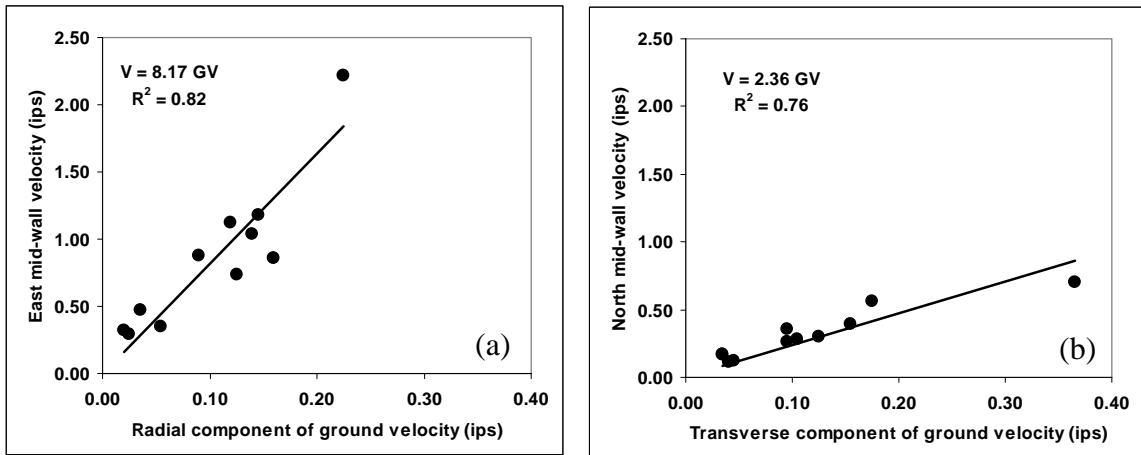


Figure 6.6 Ground velocity influence on peak mid-wall velocity for (a) radial ground velocity versus east mid-wall and (b) transverse ground velocity versus north mid-wall

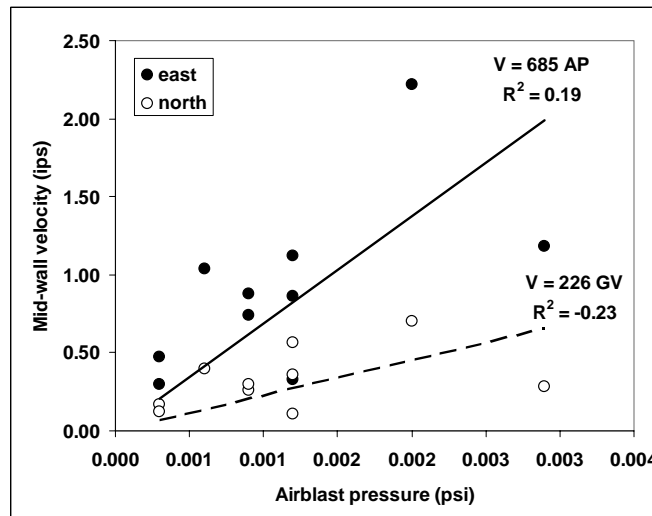


Figure 6.7 Airblast overpressure influence on mid-wall response

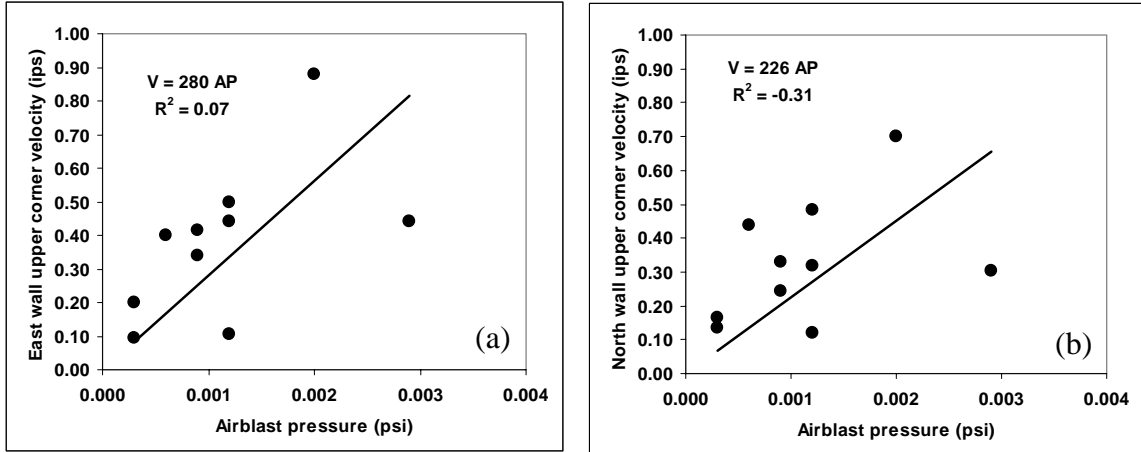


Figure 6.8 Peak airblast overpressure influence on upper structure (S2) velocity for (a) radial and (b) transverse components

Figure 6.6 shows the correlation between the peak mid-wall (MW) velocities with the peak ground velocities in the same direction. The east mid-wall response correlates best with the radial ground velocity with a correlation of 82% in comparison with 76% for the north wall. This high correlation is a result of direct excitation influence of the radial component on the east mid-wall.

Figure 6.7 examines mid-wall response to the airblast excitation rather than the ground velocity phase as in Figure 6.6. The low and the negative correlation coefficients are indicative of the lack of airblast influence on mid-wall excitation. This is because the structure response is relatively insensitive to airblast levels below 121 dB. Therefore ground motions have a higher influence on mid-wall vibrations relative to airblast.

Figure 6.8 examines the influence of airblast on the upper structure response (S2). The east wall component of the upper structure response shows a low correlation with airblast pressures, while the north wall component is negatively correlated to airblast pressures. This indicates that airblast has little or no influence on upper structure

response. This observation is consistent with massively-built, single story structures (Aimone-Martin, et al. 2003).

### 6.2.2 Natural Frequency and Damping Ratio

To compute a structure's natural frequency and damping, sufficient energy from ground motions or airblast is required. Previous studies by Aimone, et al. (2003) have shown that ground motion energy well above 0.3 ips and airblast levels above 120 dB, both at predominate frequencies near the structure's natural frequency, are required. Blasting over the time period of this study did not provide sufficient energy to reliably compute damping and natural frequency except in some cases as shown in Table 6.4. In the table damping is calculated using Equation (1).

Table 6.4 Summary of natural frequency and percentage of damping for the structure

Shot Date	Time of Blast	Natural Frequency		Damping
		Component	(Hz)	(%)
09/16/04	3:56 PM	EW	8.0	2.45
09/16/04	3:56 PM	NS	10.0	5.96
09/17/04	8:59 AM	EW	8.5	4.58
09/17/04	8:59 AM	NS	8.5	6.45
09/21/04	3:57 PM	EW	n/a	n/a
09/21/04	3:57 PM	NS	n/a	n/a
09/23/04	2:50 PM	EW	8.0	2.90
09/23/04	2:50 PM	NS	10.5	7.19
09/30/04	2:59 PM	EW	8.0	8.91
09/30/04	2:59 PM	NS	10.5	5.68
12/15/04	3:50 PM	NS	n/a	n/a
12/15/04	3:50 PM	EW	n/a	n/a
12/30/04 a	3:46 PM	EW	n/a	n/a
12/30/04 a	3:46 PM	NS	n/a	n/a
12/30/05 b	4:24 PM	NS	n/a	n/a
12/30/05 b	4:24 PM	EW	n/a	n/a
01/27/05 a	1:54 PM	EW	n/a	n/a
01/27/05 a	1:54 PM	NS	9.75	3.55
01/27/05 b	2:19 AM	EW	8.12	4.58
01/27/05 b	2:19 AM	NS	10.38	n/a
01/28/05	3:17 PM	EW	8.25	n/a
01/28/05	3:17 PM	NS	8.25	4.58

n/a – not applicable

The FFT was computed for the free response portion resulting in a structure average natural frequency of 9 Hz and is within the range of all structure types (4 to 12 Hz). The average damping ratio was computed to be 5.2% and is within the range for typical residential structures (3.5 to 13% of critical, Dowding, 1996).

### 6.2.3 Upper Structure Amplification of Ground Velocities

Table 6.5 summarizes the amplification factor (AF) calculated for the structure. The range of the AF is 1.9 to 7.6 which falls slightly above of the average range established by the U.S. Bureau of Mines and others for wood framed dwellings (0.5 to 5). This can be explained by the fact that the walls in the leaving room of the structure are far higher than normal single story houses, which make the upper structure vibrate more

Table 6.5 Summary of upper structure amplification of ground velocities

Shot Date	Time of Blast	Component	Peak Upper Structure (S2) (ips)	Corresponding Ground Motion (GV) (ips)	Amplification Factor (AF)
09/16/04	3:56 PM	EW	0.095	<0.03	n/a
09/16/04	3:56 PM	NS	-0.165	<0.03	n/a
09/17/04	8:58 AM	EW	0.105	<0.03	n/a
09/17/04	8:58 AM	NS	-0.120	<0.03	n/a
09/21/04	3:57 PM	EW	-0.340	-0.045	7.6
09/21/04	3:57 PM	NS	0.245	0.040	6.1
09/23/04	2:50 PM	EW	-0.200	<0.03	n/a
09/23/04	2:50 PM	NS	-0.135	<0.03	n/a
09/30/04	2:59 PM	EW	-0.320	-0.095	3.4
09/30/04	2:59 PM	NS	0.500	0.100	5.0
12/15/04	3:50 PM	EW	-0.485	-0.150	3.2
12/15/04	3:50 PM	NS	0.440	0.120	3.7
12/30/04 a	3:46 PM	NS	0.700	0.365	1.9
12/30/04 a	3:46 PM	EW	0.880	0.204	4.3
12/30/05 b	4:24 PM	EW	0.415	0.090	4.6
12/30/05 b	4:24 PM	NS	0.330	0.085	3.9
01/27/05 a	1:53 AM	NS	0.017	<0.03	n/a
01/27/05 a	1:53 AM	EW	0.016	<0.03	n/a
01/27/05 b	2:17 PM	EW	0.125	0.045	2.8
01/27/05 b	2:17 PM	NS	0.175	<0.03	n/a
01/28/05	3:19 PM	EW	-0.440	-0.105	4.2
01/28/05	3:19 PM	NS	-0.294	-0.080	3.7

n/a – not applicable

freely than normal structures. The average AF is computed to be 4.18. For values lower than 0.03 ips in the ground motion, the amplification factor could not be calculated, because values lower than 0,03 ips does not have influence in the structure movement.

#### 6.2.4 Strains Calculated for Structure Walls

Appendix G contains displacement time histories used to compute strains and shows the results of these strain calculations. Table 6.6 is a summary of the maximum calculated strains induced by ground motions excitation. The maximum recorded whole structure differential displacement was 0.01953 in The maximum and minimum global shear strains calculated were 135.63 and 11.94 micro-stains, respectively. The maximum in-plane tensile strain calculated was 67.44 micro-strains. This strain is compared with the strain required to cause cracking in both the exterior stucco as well as the interior gypsum drywall. According to Dowding (1985), the range of failure in the gypsum core

Table 6.6 Whole structure in-plane and mid-wall strains induced by ground motion excitation and compared with crack peak displacements

Shot Date	Maximum differential wall displacement S2-S1		Maximum shear strain		Maximum in-plane tensile strain		Maximum bending strain		Maximum ground velocity		Peak Crack Motion (micro-in)
	(in)		(micro-strains)		(micro-strains)		(micro-strains)		(ips)		
	east wall	north wall	east wall	north wall	east wall	north wall	east wall	north wall	Radial	Transverse	
09/16/04	0.00172	0.0027	11.94	18.96	5.94	5.87	3.99	2.05	0.025	0.035	735.2
09/17/04	0.00225	0.0057	15.63	39.38	7.77	12.20	4.63	1.32	0.020	0.040	249.2
09/21/04	0.00759	0.00404	52.71	28.06	26.21	8.69	12.51	5.09	0.125	0.095	776.5
09/23/04	0.00379	0.002	26.32	14.10	13.09	4.37	6.74	1.47	0.035	0.045	556.2
09/30/04	0.00980	0.00497	68.06	34.51	33.84	10.69	18.00	5.56	0.120	0.095	814.5
12/15/04	0.00707	0.00659	49.10	45.76	24.41	14.18	17.17	8.54	0.160	0.175	nd
12/30/04 a	0.01953	0.0096	135.63	66.39	67.44	30.57	38.44	14.74	0.225	0.356	2909.0
12/30/04 b	0.00803	0.006	55.76	41.94	27.73	13.00	14.78	5.27	0.090	0.125	987.0
1/27/05 a	0.00872	0.0073	60.56	50.56	30.11	15.67	16.07	5.54	0.140	0.155	1364.0
1/27/05 b	0.00258	0.0028	17.92	19.10	8.91	5.92	4.40	1.90	0.055	0.035	421.0
01/28/05	0.00817	0.00438	56.74	30.42	28.21	9.43	18.25	5.17	0.145	0.105	672.7

nd – no data

of drywall is 300 to 500 micro-strains and for stucco, failure strain occurs at 1000 micro-strains. The maximum computed tensile strain of 67.44 results in factors of safety against cracking is 4.4 for the interior drywall and 14.8 for the exterior stucco. These values are well above the safe limits of cracking. The induced strains in the structure walls never exceeded the elastic limit of the material and no permanent deformation could have occurred. Maximum bending strains computed for mid-wall flexure during the ground vibration phase of structure motions were 38.44 and 14.74 micro-strains for the east and north walls, respectively. Therefore, cracks in the exterior stucco and interior walls cannot be attributed to blasting strains.

Figures 6.9 and 6.10 show the influence of the transverse and radial ground vibrations on in-plane tensile wall strain and bending strains in mid-walls. The racking motion from the transverse ground motion shows a better correlation than that of the radial ground motion for the in-plane tensile strain, while for the bending strain both

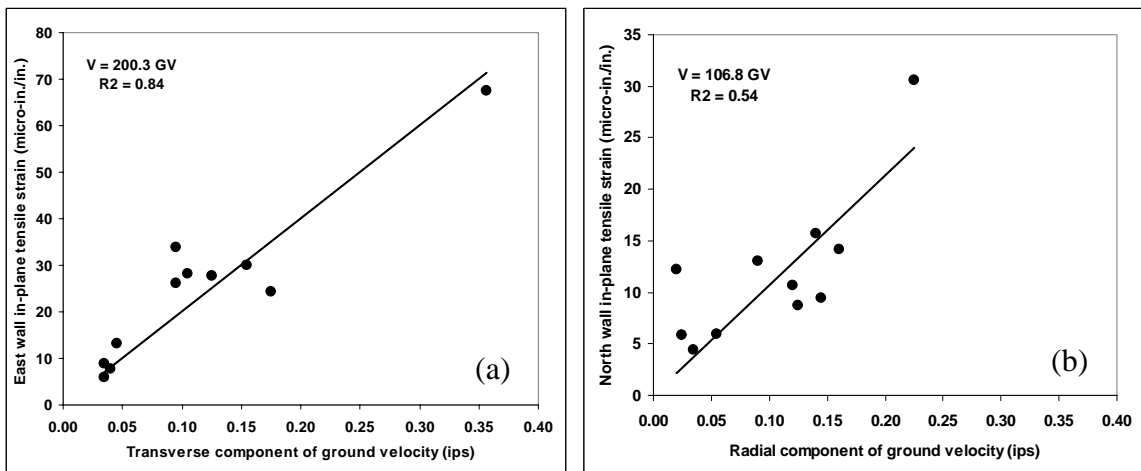


Figure 6.9 Influence of (a) transverse and (b) radial ground motions on calculated in-plane strains

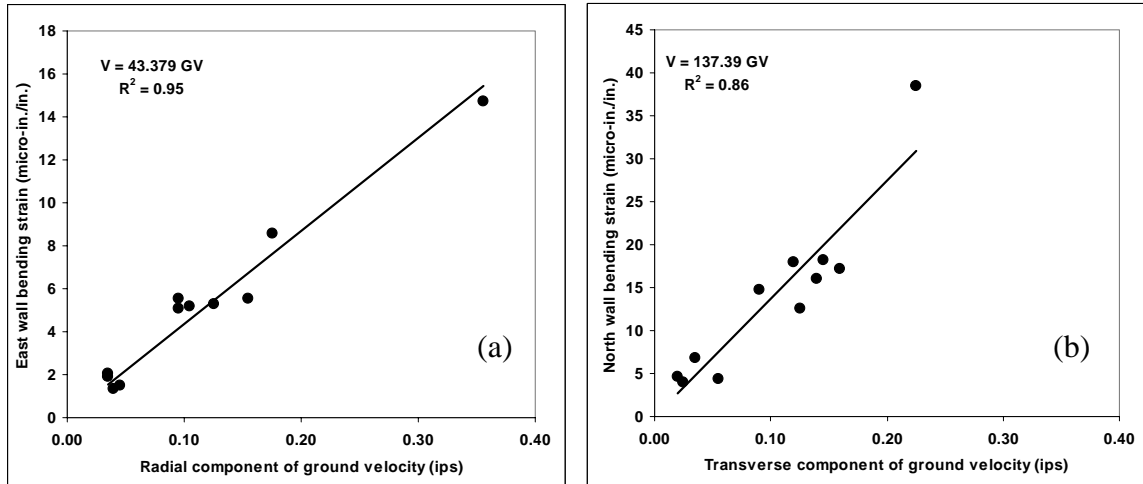


Figure 6.10 Influence of (a) radial and (b) transverse ground motions on calculated mid-wall bending strains

components show similar correlation. The differences in the correlation show that the transverse component has a higher influence in the east wall in-plane tensile strain than the radial component in the north wall. This directly affects the response of the crack in the exterior east wall. For the correlation found in the bending strain calculated for the mid-walls demonstrates that both components affect the mid-walls movement.

## 6.2.5 Crack Response

### 6.2.5.1 Environmental and Weather Induced Crack Response (long-term)

Long-term changes in crack width are presented in Figure 6.11 along with outside temperature and humidity variations for a period of 135 days (3240 hours). In general, long-term crack movement followed the trend in exterior humidity while short-term (or 24 hours) movement was consistent with diurnal temperature. When the humidity

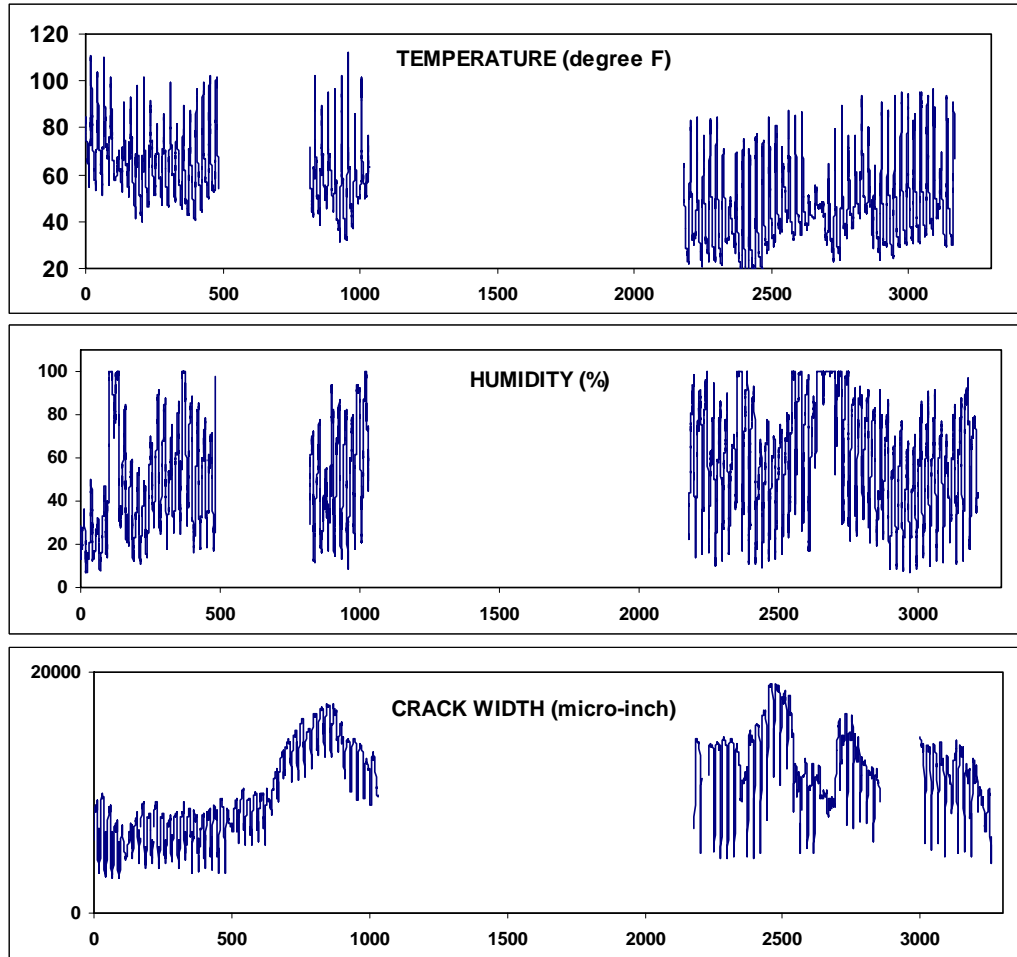


Figure 6.11 Static changes of crack width to variations in temperature and humidity over 135 days

increased, the crack opened (positive change) whereas a sudden increase in temperature produced crack closure. A portion of the crack data was lost during the study but this did not affect the quality of the remaining data.

Weather front effects such as rain, shown with the vertical dashed line in Figure 6.12, had the largest influence on long-term crack movements. In contrast, daily crack movements were strongly affected by the early morning sun on the eastern wall exposure.

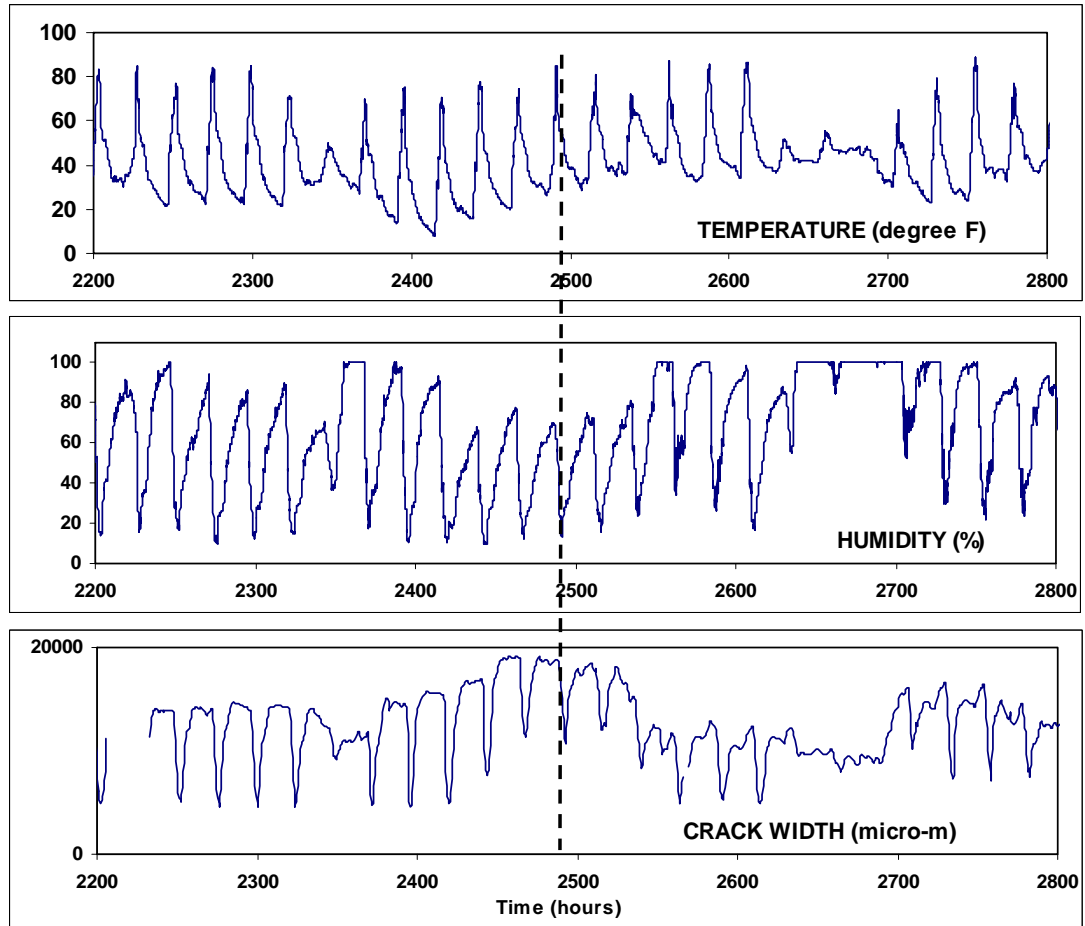


Figure 6.12 Variations in data over 22 days showing the change in crack width (positive indicated crack is opening) from early morning to mid-day

### 6.2.5.2 Crack Response to Blasting

The response of the exterior crack to changes in blasting vibrations was measured for 11 blasts events. The peak responses measured during blasting are summarized in Table 6.7. Problems with the Somat computer prevented acquiring data for some blasts. However, the dynamic crack data represents a wide range of airblast (100 to 120 decibels, dB) and ground vibrations (0.025 to 0.365 ips) amplitudes representative of the entire study.

Table 6.7 Peak crack displacement compared with ground velocity (GV), airblast, differential wall displacement (upper, S2, minus lower ,S1, structure) and mid-wall (MW) displacement

Shot Date	Radial GV Velocity (in/sec)	Trasverse GV Velocity (in/sec)	Airblast (psi)	East S1 - S2 Displacement (in)	North S1 - S2 Displacement (in)	East MW Displacement (in)	peak crack displacements (micro-in)
09/16/04	0.025	0.035	0.0003	0.00172	0.00273	0.0055	735.2
09/17/04	0.020	0.040	0.0012	0.00225	0.00567	0.0064	249.2
09/21/04	0.125	0.095	0.0009	0.00759	0.00404	0.0173	776.5
09/23/04	0.035	0.045	0.0003	0.00379	0.00203	0.0093	556.2
09/30/04	0.120	0.095	0.0012	0.00980	0.00497	0.0249	814.5
12/15/04	0.160	0.175	0.0012	0.00707	0.00659	0.0237	nd
12/30/04 a	0.225	0.365	0.002	0.01953	0.00956	0.0531	2909
12/30/04 b	0.090	0.125	0.0009	0.00803	0.00604	0.0204	987
01/27/05 a	0.140	0.155	0.0006	0.00872	0.00728	0.0222	1364
01/27/05 b	0.055	0.035	nd	0.00258	0.00275	0.0061	421
01/28/05	0.145	0.105	0.0029	0.00817	0.00438	0.0252	672.7

nd – no data

The peak dynamic crack displacement ranged from 249.2 to 2909 micro-inches across the crack. Crack gage time histories in response to blasting events are shown in Appendix H. Appendix H also contains detailed time histories for all blasts that represented both high and low amplitudes of airblast and ground motion. Crack displacement are plotted in comparison with R and T components of ground motion, airblast, and the upper corner response for the north and east walls.

Figure 6.13 shows an example of one of the composite waveforms in Appendix I for the first blast at 12/30/04 that includes the largest dynamic crack response (2909 micro-inch). As can be seen on Figure 6.13, the line between the waveforms shows that the crack motion is being driven by the transverse component of the ground motion (GV), which is parallel to the east wall, the wall that contains the crack. The transverse component of the ground motion also drives the motion in the upper structure component

located in the north wall, as can be seen in the Figure 6.13, the S2 component is slightly behind the GV peak velocity.

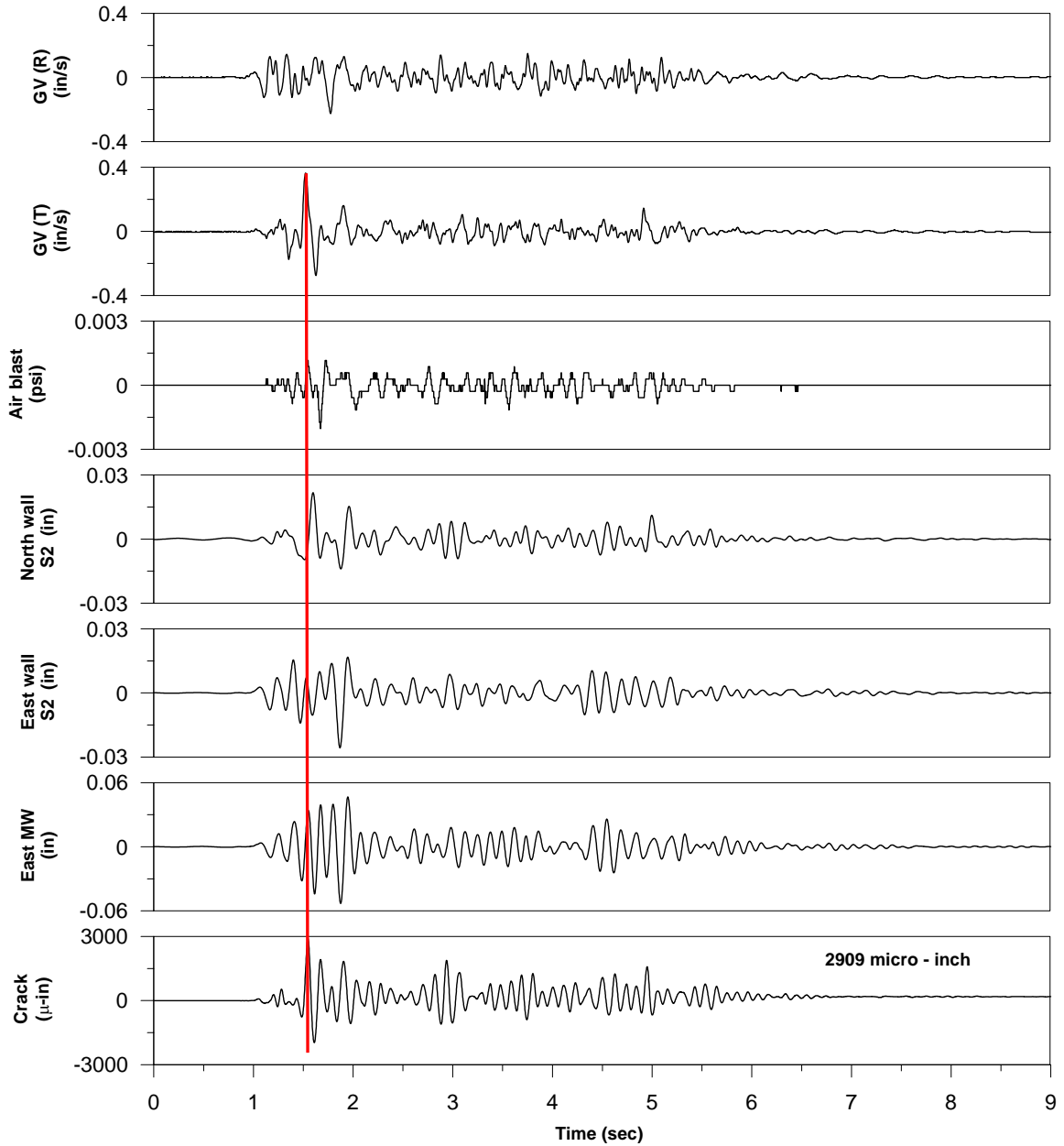


Figure 6.13 Composite waveforms, comparing crack displacement time histories with ground motion in R and T directions, airblast, upper structure east and north wall displacement and mid-wall displacement in the east wall

In Figure 6.14 (a) and (b), dynamic crack responses are compared with the maximum peak particle velocity in the radial (perpendicular) and transverse (parallel to the wall containing the crack) directions of the ground motion. In Figure 6.14 (c) and (d), dynamic crack responses are compared with maximum differential wall displacements between upper (S2) and lower (S1) transducers. Finally, in Figure 6.14 (e) peak crack responses are compared with the maximum air blast overpressures that are omnidirectional.

All plots in Figure 6.14 are time correlated, i.e., all points are the response peak (y-axes) that follows the maximum excitation peak (x-axes) by less than one period. This comparison differs from finding the maximum peak response and then finding the preceding peak excitations within the preceding response period as for amplification calculations. The distinction is important as it allows observation of the significant drivers of response.

For this structure and range of excitation frequencies, the peak particle velocity in the direction parallel with the wall containing the crack (east wall, or the transverse component of ground motion), appears to be the best predictor of the stucco crack response. Figures 6.14 (a) and (b) show that the peak crack response is not predicted at all by the maximum radial ground motions (PPV direction perpendicular to the wall containing the crack). It is the transverse motions parallel with in-plane shearing that opens and closes the crack. The next closest predictor would be the differential displacement in the direction parallel to the east wall shown in Figure 6.14 (c) and (d). However it is only a slightly better predictor than is the differential displacement in the perpendicular direction. Finally the airblast peak is the least influential in the prediction

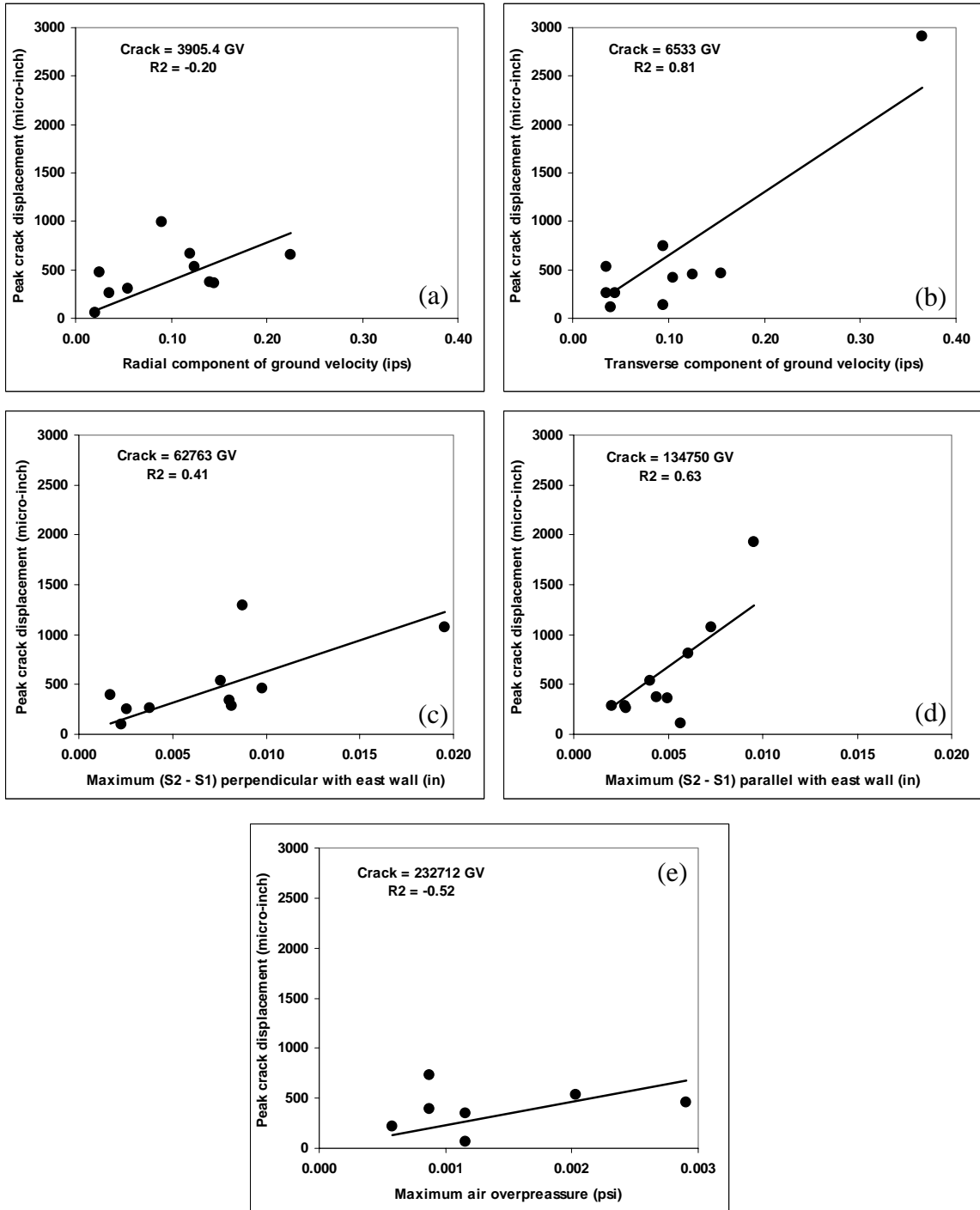


Figure 6.14 Peak dynamic crack displacement versus (a) radial and (b) transverse components of ground motions, versus maximum (S2 – S1) differential displacement (c) perpendicular and (d) parallel with east wall, and versus (e) maximum air overpressure, time correlated

of maximum crack response. The relatively small effect of the peak airblast overpressure may result from the small pressures generated at this house by these events

Daily changes in crack width over a 25-day period are compared with the dynamic crack motions for the most significant blast on 12/30/04 at 3:46 pm in Figure 6.15. The maximum daily change of 4876 micro-inch exceeded the largest change in peak-to-peak crack width during blasting (2909 micro-inches, or the difference between the highest and lowest reading about the zero amplitude line).

It is therefore concluded that the large weather-induced changes in crack width is the greatest contributing factor to crack extension and widening over time. Blasting vibration influence on changes in crack widths are negligible compared with the influence of climate. Hence, blasting is unlikely to be the source of wall cracking.

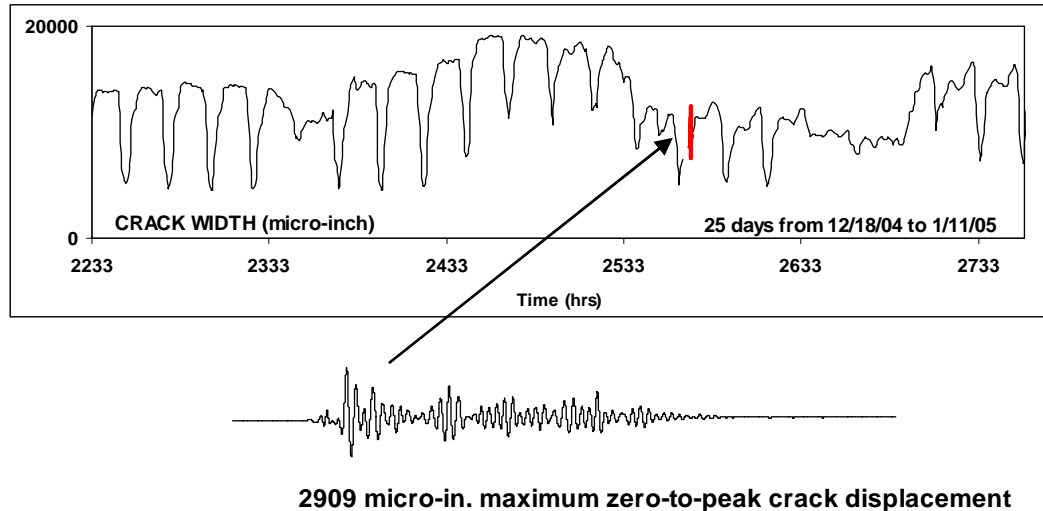


Figure 6.15 Comparison of dynamic crack displacement time history for blast on 12/30/04 with static crack movement in response to climate over a 25 day period including 12/30/04

### 6.3 Pipeline Response

To predict the response of buried pipelines to blasting, it is convenient to use velocity measurements of the ground surface for most blasting situations. Placing velocity sensors directly on the pipeline is time consuming and requires specialized instrumentation not normally available. Therefore, it is important to understand the relation between the surface response and the pipeline response for a variety of blasting practices and geologies to predict pipeline response. In general, it is well established that the amplitude of ground motion decreases with depth due to confinement. Therefore, ground near-surface velocities measurements should represent worst-case amplitudes.

The results of vibrations on the pipelines and in the ground at the monitoring stations are given in Table 6.8. Seismograph vibration report summaries for the blasts are given in Appendix C. The surface geophones were placed with the radial component oriented perpendicular with the pipeline alignment, which agree with the orientation of the single component geophones installed on the pipelines, rather than oriented to the blast initiation. The data analyzed for the pipelines was divided in two types, those blasts that were oriented perpendicular to the pipeline and those that were parallel with the pipeline, as shown in Figure 3.1.

When the pipeline was parallel with the blasts initiation, the strongest ground motion component was the transverse. When the pipelines were oriented perpendicular to the blast initiation, the strongest component was in the radial direction.

Table 6.8 Summary of vibration measurements in the pipelines

Orientation	Shot Date	Distance (ft)	Charge weight/d elay (lb)	Scaled Distance (ft/lb <sup>1/2</sup> )	RADIAL (in/sec)	Peak Frequency (Hz)	FFT Frequency (Hz)	VERTICAL (in/sec)	Peak Frequency (Hz)	FFT Frequency (Hz)	TRANSVERSE (in/sec)	Peak Frequency (Hz)	FFT Frequency (Hz)
<b>GROUND MOTION AND AIRBLAST</b>													
parallel with blast	09/21/04	110	25	22.0	<b>1.96</b>	4.3	4.12	1.06	36.5	4.06	1.46	16.0	4.09
	09/30/04	165	18.5	38.4	0.74	6.4	5.81	0.55	15.0	4.88	<b>0.84</b>	6.2	6.31
	initiation	10/07/04 b	116	48	16.7	1.36	17.0	5.06	1.62	5.3	4.88	<b>1.66</b>	11.6
perpendicular with blast initiation	10/14/04 a	57	41.5	8.8	4.72	16.0	4.00	<b>5.08</b>	19.6	4.00	4.24	19.6	12.50
	09/23/04 a	201	7.5	73.4	<b>0.15</b>	17.0	16.62	0.14	11.1	8.56	0.11	21.3	22.06
	09/23/04 b	161	5	72.0	<b>0.13</b>	21.3	16.75	0.11	18.2	9.88	0.06	25.6	15.56
	10/07/04 a	160	10	50.6	0.08	32.0	22.12	<b>0.10</b>	32.0	39.75	0.08	25.6	18.50
	10/14/04 b	136	10	43.0	0.18	25.6	22.00	<b>0.20</b>	36.5	32.25	0.18	28.4	27.75
	10/28/04	85	10	26.9	0.50	28.4	30.75	0.33	51.2	33.25	<b>0.68</b>	23.2	26.50
	<b>12 in. PIPELINE</b>												
parallel with blast	09/21/04	115	25	23.0	1.14	4.5	4.09	1.06	6.9	4.09	<b>1.28</b>	5.0	3.81
	09/30/04	165	18.5	38.4	<b>0.72</b>	7.1	5.81	0.60	5.6	5.81	0.46	6.0	6.25
	initiation	10/07/04 b	122	48	17.6	1.36	7.3	6.75	<b>1.42</b>	5.2	4.25	0.60	6.0
perpendicular with blast initiation	10/14/04 a	67	41.5	10.4	<b>2.72</b>	7.3	3.94	2.24	9.4	4.00	1.08	9.1	3.38
	09/23/04 a	196	7.5	71.6	0.11	28.4	16.62	<b>0.14</b>	28.4	8.56	0.06	28.4	10.81
	09/23/04 b	156	5	69.8	<b>0.11</b>	21.3	30.06	0.11	11.1	9.88	0.04	42.6	29.19
	10/07/04 a	158	10	50.0	0.10	51.2	22.12	<b>0.14</b>	32.0	40.75	0.09	21.3	18.50
	10/14/04 b	133	10	42.1	0.12	25.6	27.50	<b>0.19</b>	36.5	37.00	0.10	18.2	15.00
	10/28/04	88	10	27.8	0.34	51.2	39.00	0.30	42.6	39.25	<b>0.45</b>	36.5	11.50
	<b>20 in. PIPELINE</b>												
parallel with blast	09/21/04	108	25	21.6	<b>1.82</b>	10.2	4.09	1.66	5.9	4.06	1.24	4.4	3.78
	09/30/04	165	18.5	38.4	0.72	4.4	5.81	<b>0.76</b>	6.0	4.88	0.42	6.7	6.31
	initiation	10/07/04 b	110	48	15.9	2.04	13.4	9.62	<b>2.22</b>	4.0	4.88	0.74	6.9
perpendicular with blast initiation	10/14/04 a	50	41.5	7.8	5.04	11.1	12.50	<b>5.12</b>	12.8	16.25	1.44	4.4	3.38
	09/23/04 a	206	7.5	75.2	<b>0.13</b>	25.6	16.62				0.07	28.4	25.38
	09/23/04 b	60	5	26.8	<b>0.12</b>	17.0	20.31				0.05	14.2	16.56
	10/07/04 a	154	10	48.7	<b>0.15</b>	32	40.12				0.11	25.6	18.50
	10/14/04 b	131	10	41.4	nd								
	10/28/04	82	10	25.9	0.29	25.6	15.00				<b>0.64</b>	18.2	19.75

nd – no data

Figure 6.16 shows the attenuation plots of all ground motion data and compares the data with the maximum peak velocities acquired for the pipelines. The data from the pipeline falls within the rest of the attenuation data. The responses for pipelines parallel with the blast fall below at or above 50-percentile line. This is because the ground motion energy is additive and enhance by the adjacent holes detonating in line. Whereas, the blasthole detonating sequentially in a direction perpendicular to the pipeline act individually. Hence the data fall below the 50-percentile line.

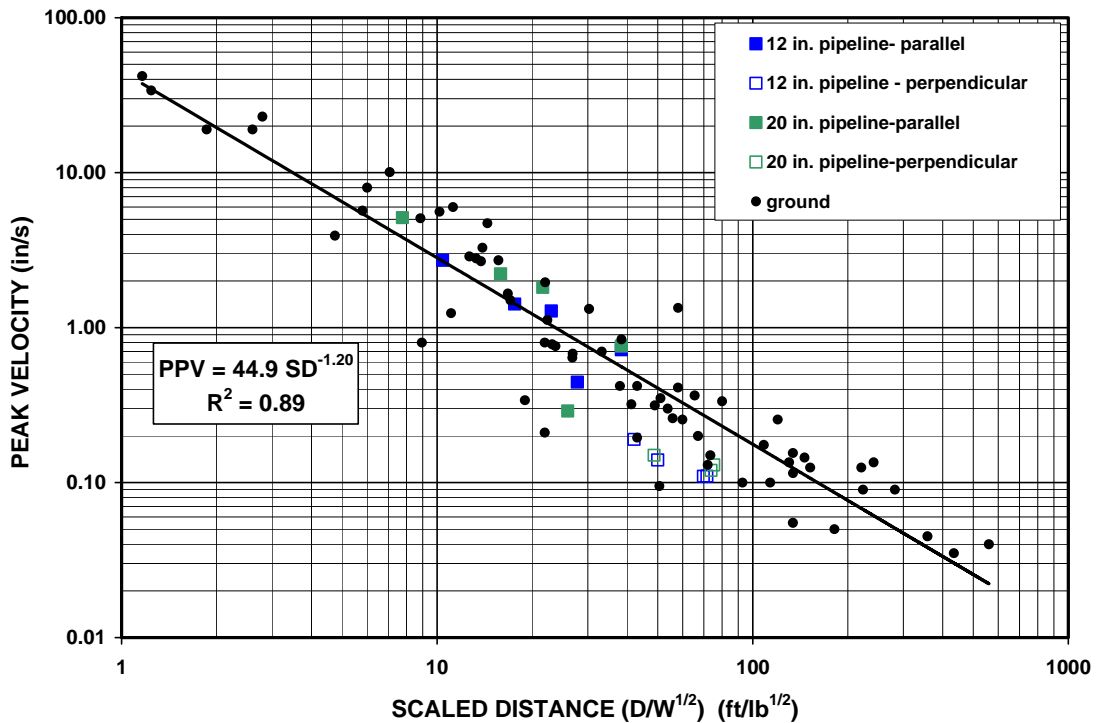


Figure 6.16 Pipeline response data plotted with the peak particle velocity of ground motion

### 6.3.1 Response of Pipelines

In Figures 6.17 through 6.19, the surface ground and pipeline response data were plotted by components, V, T, and R, respectively. The attenuation of the peak velocity in the ground is given in comparison with the maximum velocities recorded on the 12 in and 20 in pipelines for two orientations. The slope of the attenuation lines for the ground motion and pipelines are similar. This shows that the pipelines are well coupled to the ground, e.g., the vibrations from the ground couple to the pipeline.

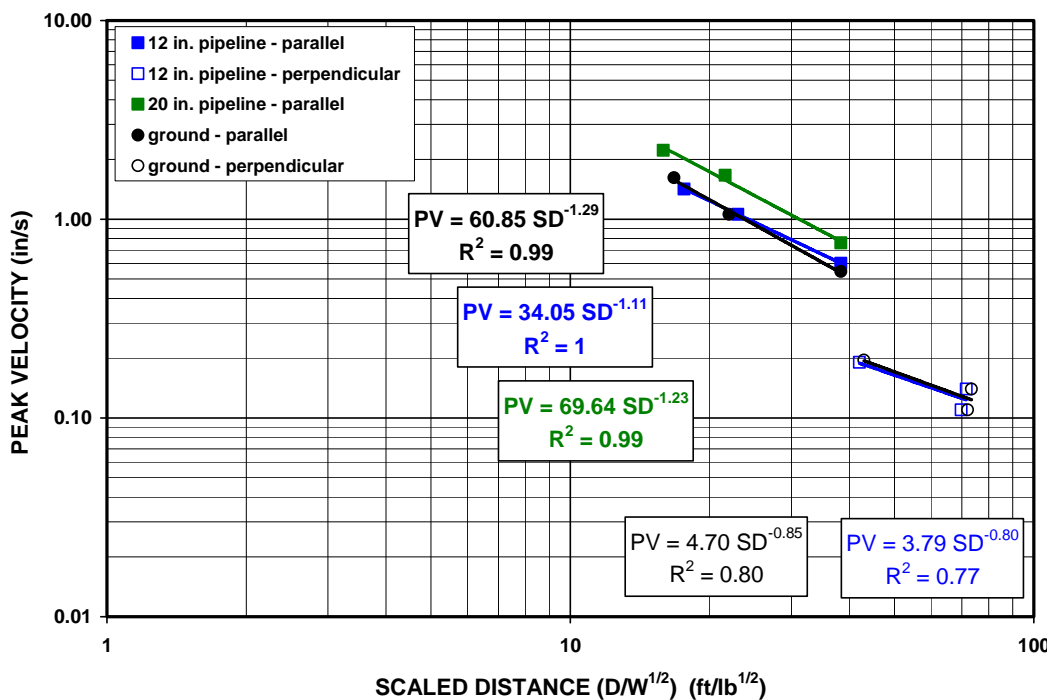


Figure 6.17 Comparison of vertical components for ground surface and pipelines grouped in respect to the orientation with the blast initiation

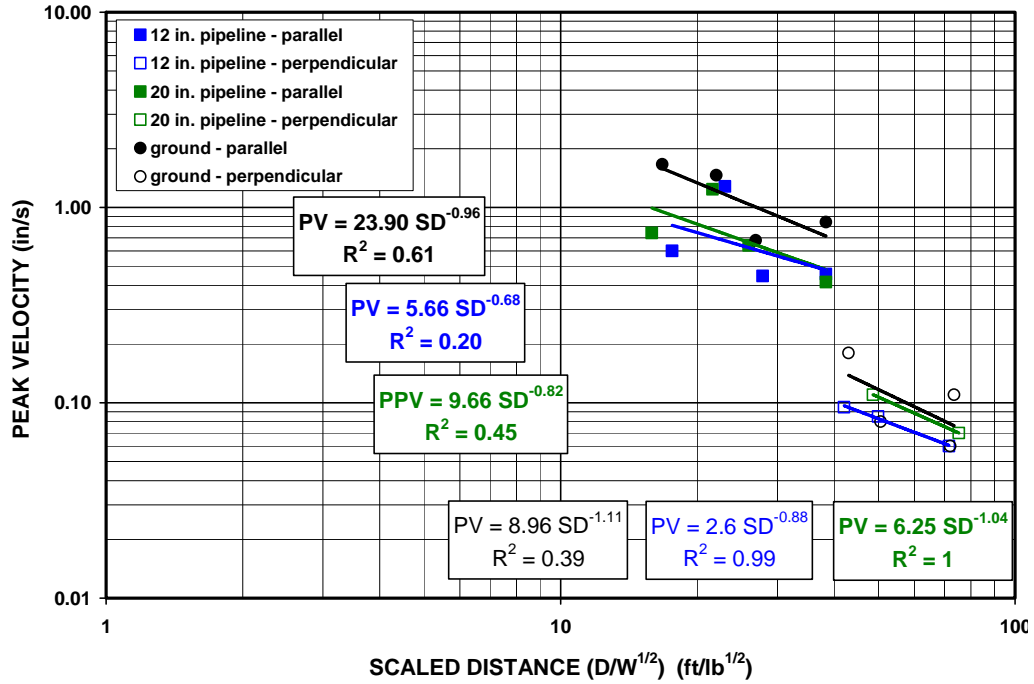


Figure 6.18 Comparison of transverse components for ground surface and pipelines grouped in respect to the orientation with the blast initiation

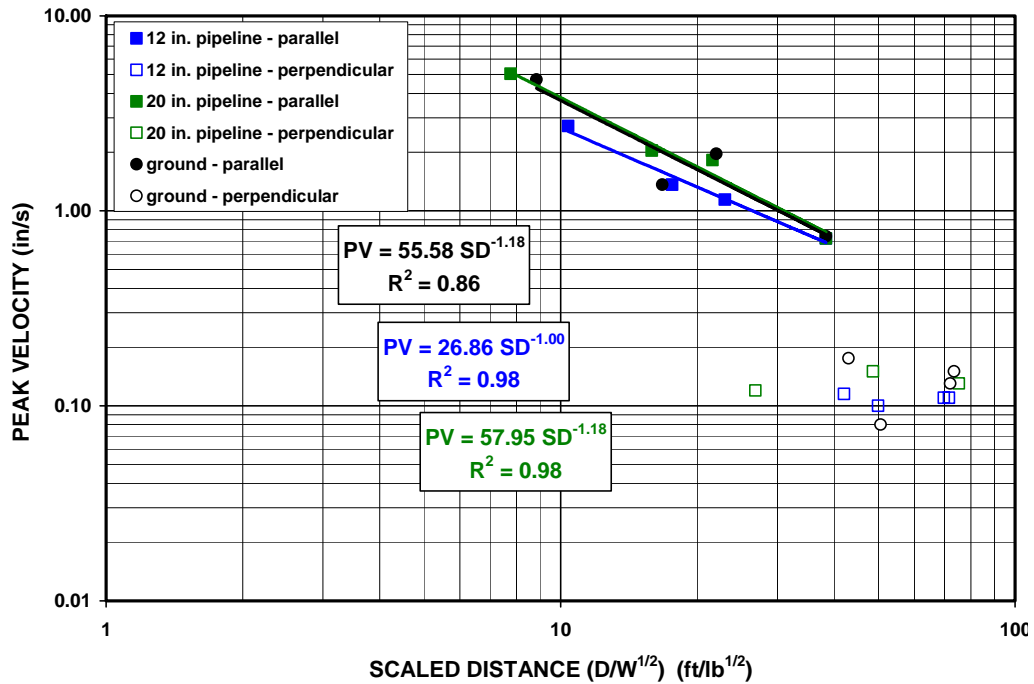


Figure 6.19 Comparison of radial components for ground surface and pipelines grouped in respect to the orientation with the blast initiation

In all cases, the K-factor for all best-fit lines is larger for the 20 in pipeline compared with the factor for the 12 in pipeline. This is because the larger diameter pipeline is more flexible, as demonstrated by the J-factor (flexibility), computed using Equation (15). Comparing the pipeline amplitudes for the parallel versus the perpendicular orientations with the blast, in the V and T cases, the parallel orientation gives a higher K-factor based on the high degree of blast wave coupling. The “K-factor for the R component is nearly constant and there is no distinction between the 20 in and 12 in pipeline responses for the blasts oriented perpendicular with the pipes. This says that the amount of bending (shown by the R component) is not affected by diameter and is perhaps related to a common wall thickness.

### **6.3.2 Response Ratio of Pipeline Relative to Ground Motion**

Table 6.9 shows the response ratio of R and V motion of the pipeline relative to the ground surface. The factor ranges, for the 12 in and 20 in pipelines, from 0.37 to 1.18 and 0.37 to 1.0 (R component), and 0.17 to 1.15 and 0.55 to 0.73 (V component). It is anticipated that the response ratios may have been higher if the pipelines had been completely buried. In any event, the pipelines were considered to be well-constrained as only a small segment of the pipeline surfaces were exposed during the study.

Table 6.9 Response ratio of pipelines relative to surface motions

Shot Date	Radial		Response Ratio	Vertical		Response Ratio
	Pipeline (ips)	Ground (ips)		Pipeline (ips)	Ground (ips)	
<b>12 in. Pipeline</b>						
09/21/04	1.14	0.420	0.37	1.06	0.180	0.17
09/23/04 a	0.11	0.150	1.36	0.14	0.120	0.86
09/23/04 b	0.11	0.090	0.82	0.11	0.030	0.27
09/30/04	0.72	0.740	1.03	0.60	0.500	0.83
10/07/04 a	0.10	0.035	0.35	0.14	0.035	0.25
10/07/04 b	1.36	1.100	0.81	1.42	1.630	1.15
10/14/04 a	2.72	1.760	0.65	2.24	np	np
10/14/04 b	0.12	0.135	1.17	0.19	0.135	0.71
10/28/04	0.34	0.395	1.18	0.30	0.240	0.81
<b>20 in. Pipeline</b>						
09/21/04	1.82	1.000	0.55	1.66	np	np
09/23/04 a	0.13	0.130	1.00	nd	np	np
09/23/04 b	0.12	0.100	0.83	nd	np	np
09/30/04	0.72	0.600	0.83	0.76	0.415	0.55
10/07/04 a	0.15	0.055	0.37	nd	np	np
10/07/04 b	2.04	1.360	0.67	2.22	1.62	0.73
10/14/04 a	5.04	np	np	5.12	np	np
10/14/04 b	nd	np	np	nd	np	np
10/28/04	0.29	0.250	0.86	nd	np	np

nd – no data

np – not possible

### 6.3.3 Estimation of Strains and Stresses in Pipelines

#### 6.3.3.1 Stress Computed from Velocity Measurements Taken on the Pipelines

The stresses in the pipelines were computed using the strain relationships of Equations (12) and (13), based on peak velocities measured for the radial and transverse components. The largest strains in bending and elongation were computed by using the highest velocities of 2.72 ips (R) and 1.28 ips (T) for the blast on 10/14/04a and 09/21/04 for the 12 in pipeline. For the 20 in pipelines, the maximum velocities were 5.04 ips (R) and 1.44 ips (T) for the blast on 10/14/04a.

The bending and longitudinal strains are computed as follows:

- Pipeline aligned parallel to the blast

12 in pipeline

$$\varepsilon_b = \frac{V_R r 2\pi f}{C_s^2} = \frac{(2.72 \text{ ips} / 12)(6 \text{ in.} / 12) 2\pi (7.3 \text{ cycles} / \text{sec})}{(996.3 \text{ ft} / \text{sec})^2} = 5.24 \mu - \text{strains}$$

$$\varepsilon_l = \frac{V_T}{C_l} = \frac{1.28 \text{ ips} / 12}{1620 \text{ ft} / \text{sec}} = 65.84 \mu - \text{strains}$$

20 in pipeline

$$\varepsilon_b = \frac{V_R r 2\pi f}{C_s^2} = \frac{(5.04 \text{ ips} / 12)(10 \text{ in.} / 12) 2\pi (11.1 \text{ cycles} / \text{sec})}{(996.3 \text{ ft} / \text{sec})^2} = 24.59 \mu - \text{strains}$$

$$\varepsilon_l = \frac{V_T}{C_l} = \frac{1.44 \text{ ips} / 12}{1620 \text{ ft} / \text{sec}} = 74.07 \mu - \text{strains}$$

- Pipeline aligned perpendicular to the blast

12 in pipeline

$$\varepsilon_b = \frac{V_R r 2\pi f}{C_s^2} = \frac{(0.34 \text{ ips} / 12)(6 \text{ in.} / 12) 2\pi (51.2 \text{ cycles} / \text{sec})}{(996.3 \text{ ft} / \text{sec})^2} = 4.59 \mu - \text{strains}$$

$$\varepsilon_l = \frac{V_T}{C_l} = \frac{0.45 \text{ ips} / 12}{1620 \text{ ft} / \text{sec}} = 23.15 \mu - \text{strains}$$

20 in pipeline

$$\varepsilon_b = \frac{V_T r 2\pi f}{C_s^2} = \frac{(0.29 \text{ ips} / 12)(10 \text{ in.} / 12) 2\pi (25.6 \text{ cycles} / \text{sec})}{(996.3 \text{ ft} / \text{sec})^2} = 1.99 \mu - \text{strains}$$

$$\varepsilon_l = \frac{V_T}{C_l} = \frac{0.64 \text{ ips} / 12}{1620 \text{ ft} / \text{sec}} = 32.92 \mu - \text{strains}$$

The hoop or circumferential strains can be estimated using the relationships developed by Siskind, et al. (1994), where

$$\varepsilon_c = 24.1 R \quad (8)$$

and R is the radial component of the surface ground motions. The 24.1 factor represents the upper envelop for all data or the worst-case estimate for  $\varepsilon_c$ . For the pipeline oriented parallel with the blast, the blasts generated R = 2.72 ips on the 12 in pipeline, and R = 5.04 ips on the 20 ips, for a corresponding surface radial component of 4.72 ips. The computed circumferential strain becomes 113.75  $\mu$  - strains. In the case of the pipelines oriented perpendicular to the blast, the blast generated R = 0.34 ips and 0.29 ips, for the 12 in and 20 in pipes respectively, with a corresponding surface radial component of 0.50 ips, and a circumferential strain of 12.05  $\mu$  - strains.

Equations (4), (5), and (6) are used to compute the hoop, longitudinal, and bending stresses in the pipe as follows:

- Pipeline aligned parallel to the blast

*12 in pipeline*

$$\sigma_c = \frac{E}{(1-\nu^2)} (\varepsilon_c + \nu \varepsilon_l) = \frac{29.5 \times 10^6}{1 - (0.292)^2} [(113.75 \times 10^{-6} + (0.292) 65.84 \times 10^{-6})] = 4,288 \text{ psi} \quad (9)$$

$$\sigma_l = \frac{E}{(1-\nu^2)}(\varepsilon_l + \nu\varepsilon_c) = \frac{29.5 \times 10^6}{1-(0.292)^2} [65.84 \times 10^{-6} + (0.292)113.75 \times 10^{-6}] = 3,194 \text{ psi} \quad (10)$$

$$\sigma_b = E\varepsilon_b = 29.5 \times 10^6 (5.24 \times 10^{-6}) = 154.6 \text{ psi} \quad (11)$$

*20 in pipeline*

$$\sigma_c = \frac{E}{(1-\nu^2)}(\varepsilon_c + \nu\varepsilon_l) = \frac{29.5 \times 10^6}{1-(0.292)^2} [(113.75 \times 10^{-6} + (0.292)74.07 \times 10^{-6})] = 4,366 \text{ psi} \quad (9)$$

$$\sigma_l = \frac{E}{(1-\nu^2)}(\varepsilon_l + \nu\varepsilon_c) = \frac{29.5 \times 10^6}{1-(0.292)^2} [74.07 \times 10^{-6} + (0.292)113.75 \times 10^{-6}] = 3,460 \text{ psi} \quad (10)$$

$$\sigma_b = E\varepsilon_b = 29.5 \times 10^6 (24.59 \times 10^{-6}) = 725.4 \text{ psi} \quad (11)$$

*- Pipeline aligned perpendicular to the blast*

*12 in pipeline*

$$\sigma_c = \frac{E}{(1-\nu^2)}(\varepsilon_c + \nu\varepsilon_l) = \frac{29.5 \times 10^6}{1-(0.292)^2} [(12.05 \times 10^{-6} + (0.292)23.15 \times 10^{-6})] = 607 \text{ psi} \quad (9)$$

$$\sigma_l = \frac{E}{(1-\nu^2)}(\varepsilon_l + \nu\varepsilon_c) = \frac{29.5 \times 10^6}{1-(0.292)^2} [23.15 \times 10^{-6} + (0.292)12.05 \times 10^{-6}] = 860 \text{ psi} \quad (10)$$

$$\sigma_b = E\varepsilon_b = 29.5 \times 10^6 (4.59 \times 10^{-6}) = 34.1 \text{ psi} \quad (11)$$

*20 in pipeline*

$$\sigma_c = \frac{E}{(1-\nu^2)}(\varepsilon_c + \nu\varepsilon_l) = \frac{29.5 \times 10^6}{1-(0.292)^2}[(12.05 \times 10^{-6} + (0.292)32.92 \times 10^{-6})] = 699 \text{ psi} \quad (9)$$

$$\sigma_l = \frac{E}{(1-\nu^2)}(\varepsilon_l + \nu\varepsilon_c) = \frac{29.5 \times 10^6}{1-(0.292)^2}[32.92 \times 10^{-6} + (0.292)12.05 \times 10^{-6}] = 1,175 \text{ psi} \quad (10)$$

$$\sigma_b = E\varepsilon_b = 29.5 \times 10^6(1.99 \times 10^{-6}) = 58.7 \text{ psi} \quad (11)$$

The highest values of the calculated hoop stress for the two pipelines from the largest blast are 4,288 psi (12 in) and 4,366 psi (20 in). These values are 1.76 and 1.73 times smaller than the recommended limit to transient loads imposed on pipelines of 7560 psi, for the X-42 pipelines, respectively, and for the X-52 these values are 2.18 and 2.14 times smaller than the recommended limit to transient loads imposed on pipelines of 9360 psi (18% of the SMYS), respectively. Furthermore, the maximum computed hoop stress is 45.5 % and 27.6 % of the maximum hoop stress of 9,400 psi and 15,800 psi resulting from the operating pressure for the 12 in and 20 in pipeline, respectively. Therefore, it is determined that all blasting that took place next to the pipelines was safe.

### **6.3.3.2 Stresses Computed from Velocity Measurements Taken on the Ground Surface**

If velocity measurements cannot be taken directly on the pipeline, velocities in the ground surface can be used to compute bending and longitudinal strains which, in turn, be used to estimate stresses induced in the buried pipeline. The strain Equations (12) and (13) are modified using the response ratio:

$$\varepsilon_b = \frac{(V_R)r2\pi f}{(1.25)C_s^2} \quad (19)$$

$$\varepsilon_l = \frac{V_T}{(1.21)C_l} \quad (20)$$

where R and T are the radial and transverse components of ground motions, and the 1.25 and 1.21 factors used are the inverse of the smallest (worst case) computed response ratios from Table 6.9. The corresponding maximum worst-case circumferential strain is computed using Equation (8).

Equations (19) and (20) were employed to estimate pipeline strains using surface ground motions above the pipelines. Stresses were then computed using Equations (9) and (10) resulting in hoop and longitudinal stresses of 5,366 psi and 6,884 psi for both pipelines. Comparisons of the predicted and computed (worst case) responses are as follows:

Stresses	Predicted	Computed	
		12 in	20 in
Hoop ( $\sigma_c$ )	5,366 psi	4,288 psi	4,366 psi
Longitudinal ( $\sigma_l$ )	6,884 psi	3,144 psi	3,460 psi

This demonstrates that the response ratio can be used to predict stresses in the pipeline, as the values for the predicted stresses are higher than those computed for the 12 in and 20 in pipes, giving a worst case scenario when compared to the recommend maximum hoop stresses. However, this method can only be used for the buried depths used in this study.

Using the elasticity equations, given above, the maximum PPV corresponding with the maximum allowable hoop stresses in the pipeline was found to be at 9.73 ips of maximum peak ground velocity. These means that at 9.73 ips of the peak particle velocity measured in the ground above the pipelines, the hoop stress in the pipes will be equivalent to the maximum allowable hoop stress, determined by the operating pressure in the pipes.

## 7 CONCLUSIONS AND RECOMMENDATIONS

The following conclusions are drawn from the structure response study:

- The lower corners (S1) for the structure compare closely with the ground velocities (GV) for the two horizontal components (T, transverse, and R, radial, shown as north and east walls, respectively), indicating good coupling of the structures with the foundations;
- The influence of airblast is negligible and does not contribute to structure shaking, except for some cases, as for the blast at 12/30/04 where it can be seen that the airblast has some influence in the increase of the mid-walls and upper (S2) motions. This is because the structure response is relatively insensitive to airblast levels below 121 dB. Therefore ground motions have a higher influence on mid-wall vibrations relative to airblast.
- Vibrations in mid-walls rarely lead to cracking but rather contribute to interior structure noise, as loose objects hanging on or leaning against walls tend to rattle with the wall motions. This rattling and resulting noise leaves persons inside a structure with the perception that structure damage is taking place.
- The FFT computed for the free response portion resulted in a structure average natural frequency of 9 Hz and is within the range of all structure types (4 to 12 Hz). The average damping ratio was computed to be 5.17% and is within the range for typical residential structures;

- The range of the amplification factor is 1.9 to 7.6 which falls slightly above the average range established by the U.S. Bureau of Mines and others for wood framed dwellings (0.5 to 5). This can be explained by the fact that the walls in the leaving room of the structure are far higher than normal single story houses, which make the upper structure vibrate more freely than normal structures;
- The maximum computed tensile strain of 67.44 results in a factor of safety against cracking of 4.4 for the interior drywall and 14.8 for the exterior stucco, and these values are well above the safe limits of cracking. The induced strains in the structure walls never exceeded the elastic limit of the material and no permanent deformation could have occurred;
- Maximum bending strains computed for mid-wall flexure during the ground vibration phase of structure motions were 38.44 and 14.74 micro-strains for the east and north walls, respectively. Therefore, cracks in the exterior stucco and interior walls cannot be attributed to blasting strains;
- The transverse component has a higher influence in the east wall in-plane tensile strain than the radial component in the north wall. This directly affects the response of the crack in the exterior east wall. The correlation found in the bending strain calculated for the mid-walls demonstrates that both components affect the mid-walls movement;
- For this structure and range of excitation frequencies, the peak particle velocity in the direction parallel with the wall containing the crack appears to be the best

predictor of the stucco crack response. The peak crack response is not predicted at all by the maximum radial ground motions. It is the transverse motions parallel with in-plane shearing that opens and closes the crack. Another predictor would be the differential displacement in the direction parallel to the east wall. However it is only a slightly better predictor than is the differential displacement in the perpendicular direction. Finally, the airblast peak is the least influential in the prediction of maximum crack response. The relatively small effect of the peak airblast overpressure may result from the small pressures generated at this house by these events;

- It is therefore concluded that the large weather-induced changes in crack width is the greatest contributing factor to crack extension and widening over time. Blasting vibration influence on changes in crack widths are negligible compared with the influence of climate. Hence, blasting is unlikely to be the source of wall cracking.

The following conclusions are drawn from the pipeline response study:

- From surface velocity measurements, the compressive wave speed was found to be 1620 ft/s, and the shear wave velocity was assumed to be 996 ft/s. This was used to compute strains in the pipelines from velocity measurements
- When the pipeline was parallel with the blasts initiation, the strongest ground motion component was the transverse, while when the pipelines were oriented

perpendicular to the blast initiation, the strongest component was in the radial direction;

- The slope of the attenuation lines for the ground motion and pipelines are similar. This shows that the pipelines are well coupled to the ground, e.g., the vibrations from the ground couple to the pipeline;
- In all cases, the K-factor for all best-fit lines is larger for the 20 in pipeline compared with the factor for the 12 in pipeline. This is because the larger diameter pipeline is more flexible, as demonstrated by the J-factor (flexibility). Comparing the pipeline amplitudes for the parallel versus the perpendicular orientations with the blast, in the V and T cases, the parallel orientation gives a higher K-factor based on the high degree of blast wave coupling;
- The response ratio of R and V motion of the pipeline relative to the ground surface ranges, for the 12 in and 20 in pipelines, from 0.37 to 1.18 and 0.37 to 1.0 (R component), and 0.17 to 1.15 and 0.55 to 0.73 (V component). It is anticipated that the response ratios may have been higher if the pipelines had been completely buried. In any event, the pipelines were considered to be well-constrained as only a small segment of the pipeline surfaces were exposed during the study.
- The highest values of the calculated hoop stress for the two pipelines from the largest blast are 4,288 psi (12 in) and 4,366 psi (20 in). These values are 1.76 and 1.73 times smaller than the recommended limit to transient loads imposed on pipelines of 7560 psi, for the X-42 pipelines, respectively, and for the X-52 these

values are 2.18 and 2.14 times smaller than the recommended limit to transient loads imposed on pipelines of 9360 psi (18% of the SMYS), respectively. Furthermore, the maximum computed hoop stress is 45.5 % and 27.6 % of the maximum hoop stress of 9,400 psi and 15,800 psi resulting from the operating pressure for the 12 in and 20 in pipeline, respectively. Therefore, it is determined that all blasting that took place next to the pipelines was safe.

- The response ratio used to estimate stresses in the pipeline gives a hoop stress of 5366 psi and a longitudinal stress of 6,884 psi., giving a worst case scenario when compared to the recommend maximum hoop stresses. These means that the response ration can be use to compute stresses in the pipeline, as the values for the predicted stresses are higher than those computed for the 12 in and 20 in pipes. However, this method can only be used for the buried depths used in this study.

Using the elastic equations to estimate the maximum peak ground velocity above the pipelines, it is recommended that the vibration levels should not be higher than 9.73 ips. This corresponds to the maximum allowable hoop stress in the pipeline (18% of the SMYS).

Further research on the geotechnical characteristics of the soil around the pipelines and structures is recommended for future studies of ground motions close to the pipelines to develop a correlation between the geology and the attenuation of the ground motions in this site. Additional analysis of the pipeline behavior to vibration using different techniques, like computer analyses and finite element modeling, to predict the stresses around and the pipes could be use to compare with the results of this study. Also

modeling to better define the response of the pipelines related to the orientation to the blast initiation, parallel with or perpendicular to the initiation, should be conducted.

## 8 REFERENCES

- Aimone-Martin, C. T., 2001, Blasting Vibration Analysis of the El Paso Natural Gas Pipeline at the McKinley Mine, Pittsburgh & Midway Coal Mining Company
- Aimone-Martin, C.T., M.A. Martell, L.M. McKenna, D.E. Siskind, and C.H. Dowding, 2003, Comparative Study of Structure Response to Coal Mine Blasting, prepared for the Office of Surface Mining Reclamation and Enforcement, Pittsburgh.
- Aimone-Martin, C.T. and K. Eltschlager, 2003. Guidelines for Measuring and Evaluating Residential Structure Response, for the Office of Surface Mining and Reclamation Enforcement, Aimone-Martin Associates, LLC.
- Dowding, C.H., 19856, Blast Vibration Monitoring and control, Prentiss-Hall
- Enron Gas Pipeline Group, 1988, Allowable Blasting Near Buried Pipelines, Engineering Standards 7155. Enron Corp., Houston, TX.
- Hitz, T. and S.D. Welsby, 1997, True Position Measurement with Eddy-Current Technology, Sensors Magazine, pp. 13.
- Mercer, M., 2002, Data Filter Software, M.S. Thesis, New Mexico Institute of Mining and Technology.

Peck, R. B., Hendron, A. J., and Mohraz, B (1972), "State of the Art of Soft Ground Tunneling," *Proceedings of the First American Rapid Excavation and Tunneling Conference*, Chicago, Society of Mining Engineers, AIME, pp. 259-286

Richard, F. E., Woods, R. D., and Hall, J. R., 1970, *Vibration of Soils and Foundations*, Prentice-Hall, Inc.

Siskind, D. E., Stagg, M.S., Kopp, J. W., and Dowding, C. H. (1980), "Structure Response and Damage Produced by Ground Vibrations from Surface Blasting," Report of Investigation 8507, U.S. Bureau of Mines, Washington, DC.

Siskind, D. E., Stagg, M. S., Wiegand, J. E., and Schulz, D. L., 1994, *Surface Mine Blasting Near Transmission Pipelines*, U.S. Bureau of Mines Report of Investigation 9523.